

Impact of the characteristics of quantum chemical databases on machine learning predictions of tautomerization energies.

Luis Itza Vazquez-Salazar,[†] Eric Boittier,[†] Oliver T. Unke,^{‡,¶} and Markus Meuwly^{*,§,||}

[†]*Department of Chemistry, University of Basel, Klingelbergstrasse 80, CH-4056 Basel, Switzerland*

[‡]*Machine Learning Group, Technische Universität Berlin, 10587 Berlin, Germany*

[¶]*DFG Cluster of Excellence “Unifying Systems in Catalysis” (UniSysCat), Technische Universität Berlin, 10623 Berlin, Germany*

[§]*Department of Chemistry, University of Basel, Klingelbergstrasse 80, CH-4056 Basel, Switzerland.*

^{||}*Department of Chemistry, Brown University, Providence RI, USA*

E-mail: m.meuwly@unibas.ch

Abstract

An essential aspect for adequate predictions of chemical properties by machine learning models is the database used for training them. However, studies that analyze how the content and structure of the databases used for training impact the prediction quality are scarce. In this work, we analyze and quantify the relationships learned by a machine learning model (Neural Network) trained on five different reference databases (QM9, PC9, ANI-1E, ANI-1 and ANI-1x) to predict tautomerization energies from molecules in Tautobase. For this, characteristics

such as the number of heavy atoms in a molecule, number of atoms of a given element, bond composition, or initial geometry on the quality of the predictions are considered. The results indicate that training on a chemically diverse database is crucial for obtaining good results but also that conformational sampling can partly compensate for limited coverage of chemical diversity. The overall best performing reference database (ANI-1x) performs on average by 1 kcal/mol better than PC9 which, however, contains about two orders of magnitude fewer reference structures. On the other hand, PC9 is chemically more diverse by a factor of ~ 5 as quantified by the number of atoms it contains compared with the ANI family of databases. We explicitly demonstrate that when certain types of bonds need to be covered in the target database (Tautobase) but are undersampled in the reference databases the resulting predictions are poor. Examples include $C(sp^2)-C(sp^2)$ double bonds close to hetero atoms and azoles containing N-N and N-O bonds. A quantitative measure for these deficiencies is the Kullback-Leibler divergence between reference and target distributions. Analysis of the results with a TreeMAP algorithm provides deeper understanding of specific deficiencies in the reference data sets. Capitalizing on this information can be used to either improve existing databases or to generate new databases of sufficient diversity for a range of ML applications in chemistry.

April 14, 2021

1 Introduction

In the last decade, the application of machine learning (ML) techniques in chemistry has significantly increased.¹⁻⁴ This has occasionally been related to a paradigm shift, revolutionizing the available techniques to understand and simulate chemistry.^{5,6} The excitement is seemingly justified, given the outcomes of ML techniques' central promise that, by using a sufficiently large number of examples and a rule-discovery algorithm, it is possible to obtain a scientific understanding of the underlying relationships covered by the data.^{1,3} Furthermore, ML techniques are fast compared with quantum chemical methods, while also reaching comparable accuracy.⁷⁻¹⁷

On the other hand, application of quantum ML methods to concrete problems requires large amounts of data which first need to be generated from electronic structure calculations.^{18–20} Consequently, data generation is computationally demanding. An essential challenge for the extension of ML methods' applicability in chemistry is understanding how suitable databases can be constructed to maximize accuracy and transferability of the models. An important ingredient for this step is the degree and confidence with which a human can understand the relationship between cause (starting database and model) and result or observation (applying the model to a new task).^{21,22} This process has also been called “interpretability” and it can be used to understand the relationships learned by the model or contained in the data used for training it.^{23,24} Part of the present work is concerned with the aim to relate the composition of the initial chemical databases based on which ML models are conceived with their performance on the prediction of a property of interest (tautomerization energy) on a set of unseen examples.

To test the effect of different databases on the reliability of the ML model, the problem of predicting tautomerization energies is considered. Tautomerism is a form of reversible isomerization involving the rearrangement of a charged leaving group within a molecule²⁵ (e.g. Fig. 1a). One isomer transforms into the other by a heterolytic splitting followed by a recombination of the fragments formed.²⁶ This process involves the migration of one or more double bonds and atoms or groups. The isomers (i.e. tautomers) generated in this reaction are chemically independent species with defined properties.²⁷ It is known that this type of reaction is of importance for biological molecules such as amino acids,²⁶ DNA,^{28,29} RNA,³⁰ and atmospheric processes.³¹ Additionally, it is estimated that tautomerism can occur in up to two thirds of small molecules,³² and a majority of commercial drugs.^{33,34}

Despite its widespread occurrence and importance, quantitative studies of tautomerism are still challenging because small changes in molecular structure or solvent environment can dramatically change the tautomeric equilibrium.^{27,35} Moreover, small free energy differences between

two tautomers in solution make the use of high level theoretical methods and an adequate basis set mandatory which limits its use for calculations of tautomerization energies and ratios.^{35,36} As an example, tautomerization in malonaldehyde (MA) is considered. MA has served as a prime example to develop and test computational methods for a realistic description of hydrogen transfer in small molecules.³⁷ Experimentally, the ground state tunneling splitting is 21.58314 cm^{-1} which has been determined by different experiments with very high accuracy.^{38,39} Furthermore, proton transfer rates in a di-imine derivative have been determined with nuclear magnetic resonance (NMR) spectroscopy.⁴⁰ Such experiments provide direct information on the barrier height separating the two tautomeric states “A” and “B”. Using a state-of-the art full-dimensional potential energy surface at the near basis-set-limit frozen-core CCSD(T) level of theory,⁴¹ the tunneling splitting from quantum simulations was determined as 23.4 cm^{-1} .⁴² Alternatively, using a reduced dimensionality Hamiltonian, the barrier height for proton transfer in a parametrized molecular mechanics with proton transfer (MMPT) potential was found to be 4.34 kcal/mol which yields a tunneling splitting of 21.2 cm^{-1} , consistent with experiment.^{43,44} This barrier height is close to the value from CCSD(T) calculations which yield 4.1 kcal/mol .⁴¹ These examples illustrate that calculations at the highest levels of theory are required for quantitative studies of the energetics underlying tautomerization.

In the last decade, development of ML models has allowed the design of robust models that can routinely reach prediction errors better than chemical accuracy at low computational cost.^{12,45} However, there have been few discussions on how databases can be improved/adjusted to obtain better predictions from the ML model. Ideally, the combination of a robust ML model and an adequate database will result in quantitative results for the prediction of a property of interest. The availability of public databases of tautomers^{46,47} makes the prediction of tautomerization energies using these ML models an ideal test case to study how different training databases influence the accuracy of ML methods.

The present work is structured as follows. First, the methods, databases, and the analysis performed are introduced. Next, the results for the tautomerization energy predictions using models trained on the different tested databases are presented. Additionally, prediction errors for tautomerization energies are analyzed. The effect of different characteristics of the training data on predicting the tautomerization energy and the individual molecules' energy are evaluated. Finally, the results are discussed and conclusions regarding the findings and interpretability of broadly conceived and learned ML models applied to a specific chemical question are drawn.

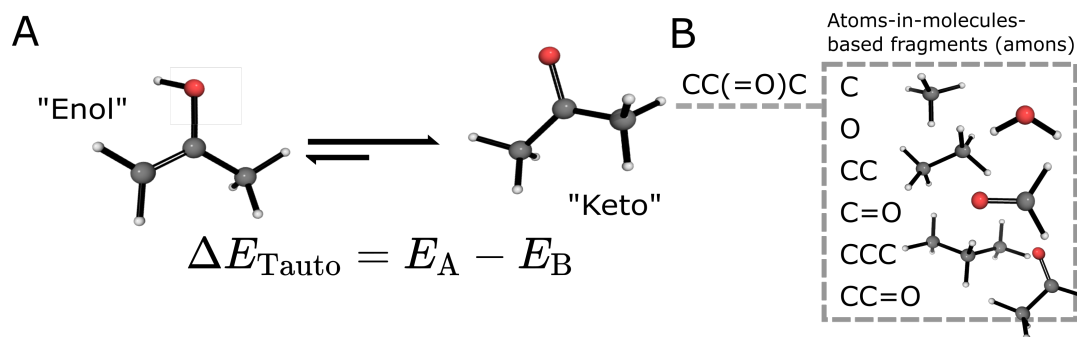


Figure 1: (A) Tautomerism is a form of reversible isomerization involving the rearrangement of a charged leaving group within a molecule. The keto-enol tautomerism of acetone, an equilibrium which heavily favours the keto side, is shown as an example. (B) Chemical space can be decomposed systematically through the use of atoms-in-molecules-based fragments (amons).⁴⁸ The amons present in acetone (SMILES: CC(=O)C), as well as their corresponding SMILES are given as an example.

2 Methods

2.1 Machine Learning

PhysNet was used for the representation and evaluation of the data sets, using the hyperparameters from the original publication.⁴⁵ For training, only the nuclear charges (Z), the energies of the molecules (E) and their coordinates (\mathbf{R}) were considered. The energies used for training were those reported by the different databases minus the atomization energy at the given level of theory.

In all cases, a training, testing and validation split of 8 : 1 : 1 was used. The loss function was

$$\mathcal{L} = w_E |E - E^{\text{ref}}| + \lambda_{\text{nh}} \mathcal{L}_{\text{nh}} \quad (1)$$

where E^{ref} is the reference energy, $w_E = 1$ is the weighting hyperparameter for the energy, $\lambda_{\text{nh}} = 10^{-2}$ is a regularization hyperparameter and the term \mathcal{L}_{nh} is a non hierachicality regularization penalty. The loss function (Eq. 1) was minimized using AMSgrad with a learning rate of 10^{-3} . Overfitting was prevented by the use of early stopping, the convergence criteria considered is the saturation of the validation-loss function.⁴⁵

2.2 Database Selection

For training the NNs, four widely used databases for benchmarking predictive models of DFT-based energies are employed, namely QM9,⁴⁹ PC9,⁵⁰ ANI-1⁵¹ and ANI-1x.⁵² An additional database, ANI-1E (where "E" stands for equilibrium) containing only the equilibrium structures of the ANI-1 database, was generated at the ω B97x/6-31G(d) level of theory. These databases can be divided into categories based on the type of geometries they contain. The datasets consisting solely of equilibrium structures are QM9, PC9 and ANI-1E, and sample only chemical space. Contrary to that, the ANI-1 and ANI-1x databases contain equilibrium and non-equilibrium structures which sample chemical and conformational space.

Training sets: The QM9 data set⁴⁹ was generated as a subset of the GDB-17 chemical universe,⁵³ consisting of 133885 molecules, containing less than or equal to 9 heavy atoms (either C, N, O or F). Reference energies were computed at the B3LYP/6-31G(2df,p) level of theory. For the present work, QM9 was filtered to include only molecules which passed a geometry consistence check⁴⁹ and considering only those containing carbon, nitrogen or oxygen atoms. The final size of the QM9 training dataset used here consisted of 110426 molecules.

The PC9 dataset was created as an alternative to QM9 to improve coverage of chemical space.⁵⁰ It is a subset of the PubChemQC⁵⁴ and is limited to molecules with 9 heavy atoms or less ($n_{\text{atoms}} \leq 9$). This database consists of 99234 molecules, calculated at the B3LYP/6-31G(d) level of theory, and excludes enantiomers, tautomers, isotopes as well as other specific artifacts in PubChemQC.⁵⁰ PC9 also contains 5325 molecules with an electronic state different from a singlet which were removed for the present work. As in the case of QM9, molecules which contain fluorine were removed. The final size of this dataset was 85875 molecules.

ANI-1⁵¹ consists of 24 million geometries generated using normal mode sampling from 57462 unique molecules. ANI-1 is a subset of the GDB-11 chemical universe.^{55,56} A related dataset, ANI-1x,⁵² was created using an active learning⁵⁷ procedure which reduced the original ANI-1 database to 5 million structures. Starting from the ANI-1 database^{51,58} the ANI-1E dataset was generated and consists only of the corresponding equilibrium structures. The new ANI-1E database contains 57462 molecules limited to eight heavy atoms (either C, O or N). The generation of this database is further described below in the subsection of electronic structure calculations.

Tautomerization energy evaluation set: The performance of the NN models described above was evaluated on a subset of molecules from TautoBase,⁴⁶ a public database of 1680 tautomer pairs. The Tautobase was filtered to molecules only containing hydrogen, carbon, nitrogen, or oxygen atoms. The size of the final test set was 1257 tautomer pairs (2514 molecules). The geometry generation and structural optimization for these molecules is described below.

2.3 Initial geometry

To investigate the effect of the geometry of the molecules passed to the NN model on its performance, a second set of geometries for the tautobase was also evaluated. These geometries

were generated from the SMILES representation using OpenBabel⁵⁹ and were optimised with the MMFF94 force field.⁶⁰

Additionally, a subset of the test set composed of 34 tautomeric pairs which were part of the SAMPL2 challenge⁶¹ were considered. Those 34 pairs (68 molecules) were optimized by six popular general atomistic force fields: CHARMM27,⁶² GAFF,⁶³ OPLS,⁶⁴ UFF,⁶⁵ Gromos,⁶⁶ and Ghemical.⁶⁷ Details on the generation of the geometries are reported in the SI.

2.4 Electronic Structure Calculations

Generation of ANI-1E: Starting from the ANI-1 database,⁵⁸ a new data set, ANI-1E, was generated. From the SMILES strings provided by Smith et al.⁵⁸ initial geometries using OpenBabel⁵⁹ were generated. Subsequently, geometries were optimised using PM7⁶⁸ implemented in MOPAC2016,⁶⁹ before a final geometry optimization and frequency calculation at the ω B97x/6-31G(d) level of theory was performed using Gaussian09.⁷⁰ The final results were checked to assure they did not contain imaginary frequencies and therefore correspond to minima on the potential energy surface.

Tautomerization evaluation set: The molecules used for the evaluation of the NN models were generated from the SMILES provided in Ref. 46 using the OpenBabel software.⁵⁹ These structures were then optimized at the same level of theory for each of the databases used for training (QM9: B3LYP/6-31G(2df,p), PC9: B3LYP/6-31G(d), ANI: ω B97x/6-31G(d)) using Gaussian09.⁷⁰ Here, the tautomerization energy ΔE_{Tauto} is defined as the energy difference between tautomers A and B in their optimized structures, see Figure 1. These optimized geometries were given as input to the respective, previously trained NN models using the five reference databases QM9, PC9, ANI-1E, ANI-1 and ANI-1x.

Table 1: Overview of the training datasets used in this work. QM9, PC9 and ANI-1E contain equilibrium structures and can be considered to only sample chemical space, whereas ANI-1 and ANI-1x also contain non-equilibrium geometries which sample conformational space. The number of molecules refers to the total number of data in each dataset.^aStructures generated through normal mode sampling. ^bTraining set selected using active learning.

| Database | Number of Molecules | Level of Theory | Parent Universe |
|---------------------|---------------------|------------------------|-----------------|
| QM9 | 128908 | B3LYP/6-31G(2df,p) | GDB-17 |
| PC9 | 85870 | B3LYP/6-31G(d) | PubChemQC |
| ANI-1E | 57462 | ω B97x/6-31G(d) | GDB-11 |
| ANI-1 ^a | 24 million | ω B97x/6-31G(d) | GDB-11 |
| ANI-1x ^b | 5 million | ω B97x/6-31G(d) | ANI-1 |

2.5 Comparison of structural properties of different databases

As a way to compare the composition of the different datasets evaluated in terms of structural properties (e.g. bond lengths), a Gaussian kernel density estimation⁷¹ of their distributions was generated, see Figures ?? to ??. The similarities between the distributions used to train the NN models and those from the test set of tautomers was quantified by computing the relative entropy (or Kullback-Leibler (KL) divergence)⁷²

$$D(p \parallel q) = \int_{-\infty}^{\infty} p(x) \log \left(\frac{p(x)}{q(x)} \right) dx \quad (2)$$

This metric quantifies the overlap between a reference distribution $p(x)$ and a target distribution $q(x)$. Because the KL divergence is not symmetric ($D(p \parallel q) \neq D(q \parallel p)$), it is important to specify which distribution is used as the reference. In the present work, the Tautobase (target) distribution and the QM9, PC9, ANI-1E are the reference distributions. The KL divergence allows to quantify how much information of the reference databases (i.e. QM9, PC9, ANI-1E) is 'missing' to best cover the information contained in Tautobase.

2.6 Chemical Space “Coverage” from Fragment Analysis

The ‘coverage’ of chemical space contained in the Tautobase, QM9, PC9 and ANI family of databases was analysed with respect to the atom-in-molecule-based fragments (amons).⁴⁸ The amons are generated from the SMILES representation of the molecule, see Figure 1b. This representation is used to construct a molecular graph from which sub-graphs to a maximum number of atoms (excluding hydrogen) are generated. All sub-graphs are checked to be valid and unique. Here, amons up to and including a maximum of five heavy atoms were generated by an in-house script.

3 Performance of the NN on the Tautobase

3.1 Overall Performance

The mean absolute errors for the tautomerization energies ΔE_{Tauto} range from 1.68 kcal/mol (ANI-1x) to 4.59 kcal/mol (ANI-1). The results are summarized in Table 2 for all molecules in the test set and graphically reported in Figures 2 (datasets with equilibrium structures) and 3 (datasets with both equilibrium and non-equilibrium structures). The prediction errors for the energy of single isomers, E_{SI} , with respect to DFT energies are also reported (Table 2). Note that because the tautomerization energy is defined as the difference between the isomer energies, predictions of tautomerization energies are often more accurate due to cancellation of systematic errors. On the other hand, the energies for single isomers are considerably larger and span a much wider range because they scale with the number of atoms that make up a molecule. Therefore, the NN-based energies for larger molecules are expected to be associated with considerably larger errors.

To assess whether the accuracy for predicting tautomerization energies correlates with the performance of the trained NNs on the chemical databases, the QM9, PC9, and ANI-1E models are considered. The MAEs on held-out test sets for each of the respective training runs are 0.10 kcal/mol

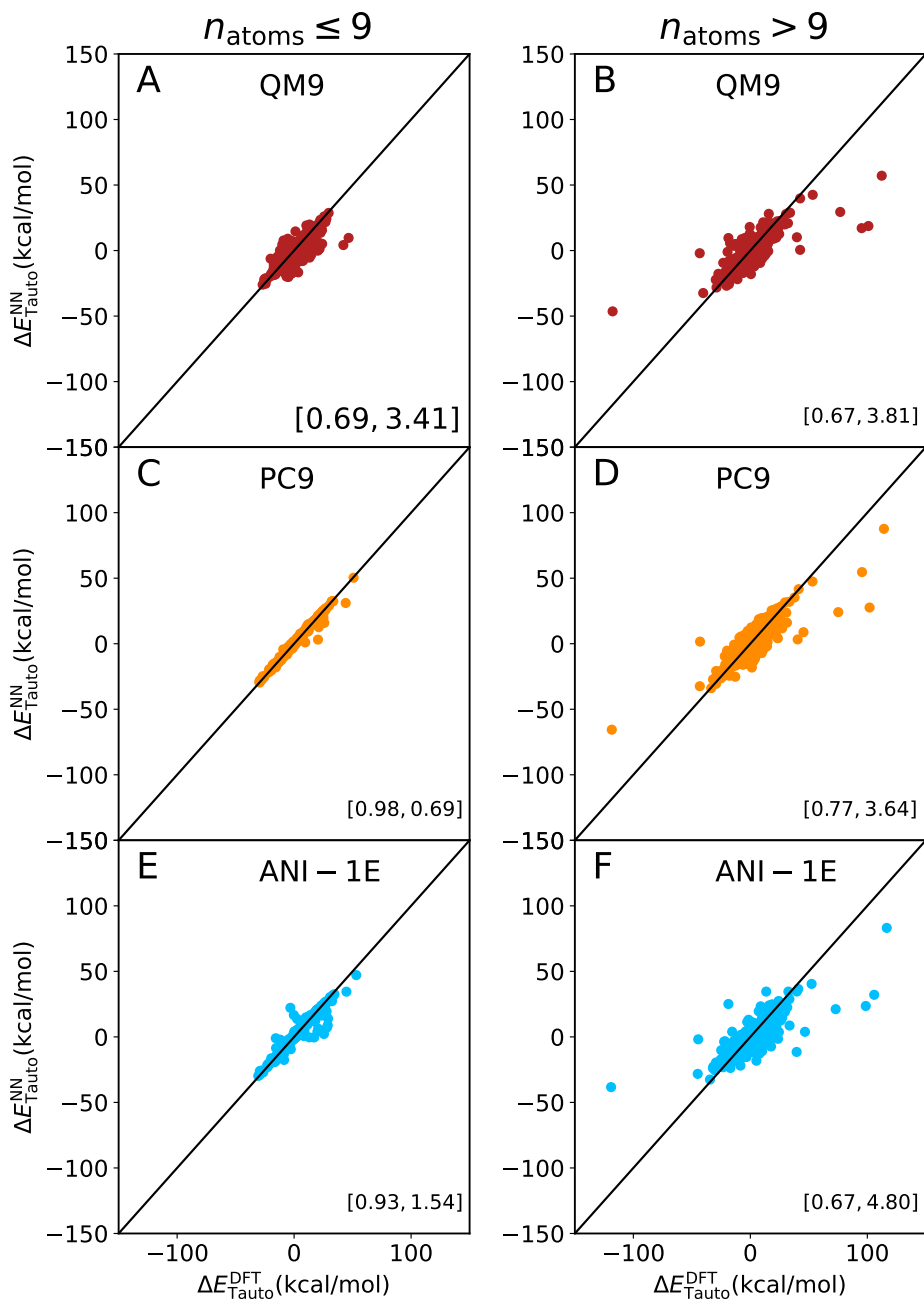


Figure 2: Correlation between the calculated (DFT) and predicted (NN) tautomerization energies ($\Delta E_{\text{Tauto}} = E_A - E_B$) for molecules with $n_{\text{atoms}} \leq 9$ (left) and $n_{\text{atoms}} > 9$ (right) for the models trained on the datasets which only cover chemical space. Pearson correlation coefficients (r^2) and the Mean Absolute Error (MAE) values are reported in brackets as [r^2 , MAE].

(QM9), 0.69 kcal/mol (PC9), and 0.27 kcal/mol (ANI-1E) which is comparable to values ranging from 0.19 kcal/mol to 0.30 kcal/mol for the QM9 data set (depending on the sizes of the training and validation sets used).⁴⁵ However, when applying these trained NNs to evaluate Tautobase,

the MAEs are 3.67 kcal/mol (QM9), 2.60 kcal/mol (PC9), and 3.66 kcal/mol (ANI-1E), respectively. Hence, there appears to be no correlation between the quality of the trained NNs (measured on test data sampled from the same database used for training) and their performance on Tautobase.

Table 2: Mean Absolute (MAE) and Root-Mean-Squared Error (RMSE) for the prediction of tautomerization energy ΔE_{Tauto} , and the single isomer energies, E_{SI} , for the entire Tautobase (1257 tautomeric pairs) for each of the datasets.

| Database | ΔE_{Tauto} | | E_{SI} | |
|----------|---------------------------|------|-----------------|-------|
| | MAE | RMSE | MAE | RMSE |
| QM9 | 3.67 | 7.12 | 5.00 | 8.40 |
| PC9 | 2.60 | 5.41 | 6.90 | 13.20 |
| ANI-1E | 3.66 | 7.09 | 15.20 | 17.50 |
| ANI-1 | 4.59 | 7.56 | 13.40 | 17.00 |
| ANI-1x | 1.68 | 2.85 | 1.80 | 3.60 |

Next, the performance of the trained models for predicting ΔE_{Tauto} and E_{SI} depending on the number of heavy atoms is assessed. For this, results for the subset of molecules with $n_{\text{atoms}} \leq 9$, referred to as ‘‘Set1’’ in the following, is considered separately from those with $n_{\text{atoms}} > 9$, which is ‘‘Set2’’. This distinction is motivated by the fact that the PC9 and QM9 databases contain structures with only up to 9 heavy atoms, i.e. models need to extrapolate for larger structures. For Set1, the PC9 (Figure 2C) and ANI-1x (Figure 3C) data sets perform best. Both achieve chemical accuracy (MAE < 1 kcal/mol) with respect to the DFT values for ΔE_{Tauto} .

The extrapolation to Set2 increases the prediction errors for most of the databases studied. Again, the ANI-1x database performed best for ΔE_{Tauto} with a MAE of 2.20 kcal/mol, followed by PC9, QM9, ANI-1E and ANI-1 with a MAE of 6.29 kcal/mol. The number of atoms in the database also influences the correlation coefficient r^2 . A better correlation is observed when the size of evaluated molecules is in the range covered by the training database, i.e. for Set1. Here, the correlation coefficients range from 0.69 (QM9) to 0.99 (ANI-1x). For Set2, the r^2 values are significantly lower. A particularly noteworthy case is the QM9 database, which shows almost the same MAE and r^2 for

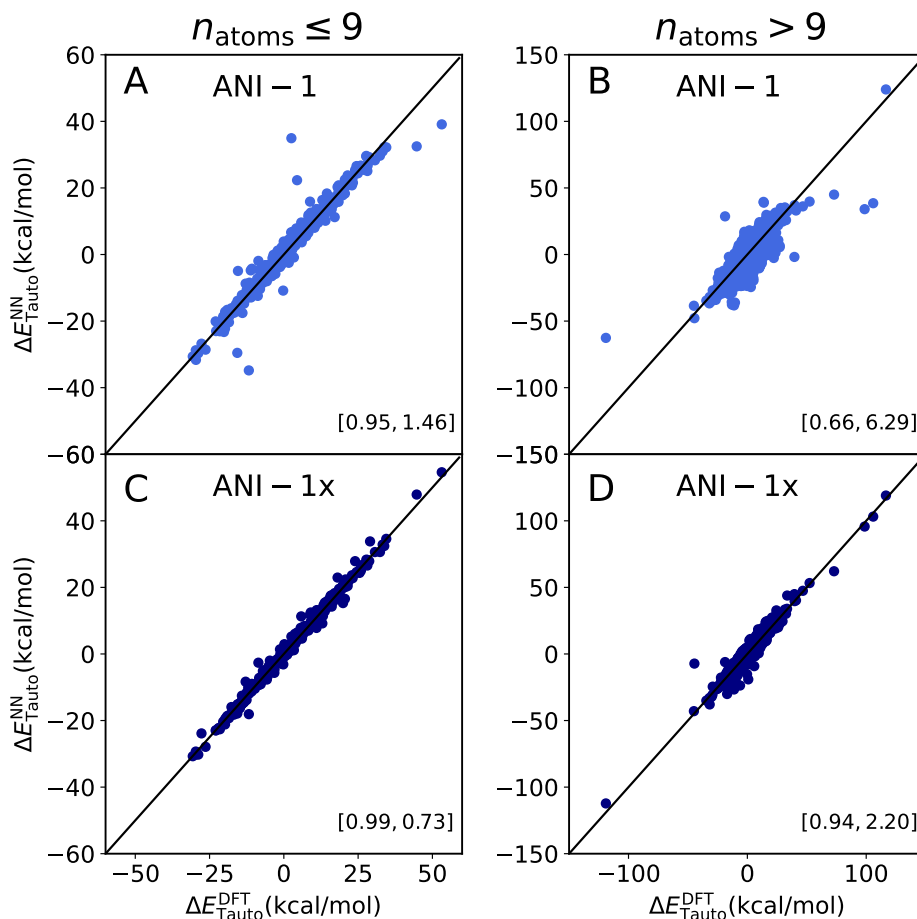


Figure 3: Correlation between the calculated (DFT) and predicted (NN) tautomerization energies ($\Delta E_{\text{Tauto}} = E_A - E_B$) for molecules with $n_{\text{atoms}} \leq 9$ (left) and $n_{\text{atoms}} > 9$ (right) for the models trained with the datasets which cover chemical and conformational space. Pearson correlation coefficients (r^2) and Mean Absolute Error (MAE) values are reported in brackets [r^2 , MAE].

both subsets of the tautobase (Figures 2A and B). The performance for Set1 and Set2 also differs in the number and magnitude of outliers, see Figures 2 and 3.

The RMSE in Table 2 show that the spread for E_{SI} could be a reason for large outliers (see Figure ??). It is likely that there is some error cancellation when predicting tautomerization energies (i.e. energy differences). For example, if the trained NN predicts too large energies for both isomers, this systematic error cancels when their energy difference is computed.

3.2 Error analysis

Next, prediction errors for ΔE_{Tauto} and E_{SI} are analyzed and discussed for all trained models. In Figures 4A and B, the kernel density estimate of the error distribution is reported. The violin plots in Figures 4C and D show the spread of errors, which helps to identify large outliers.

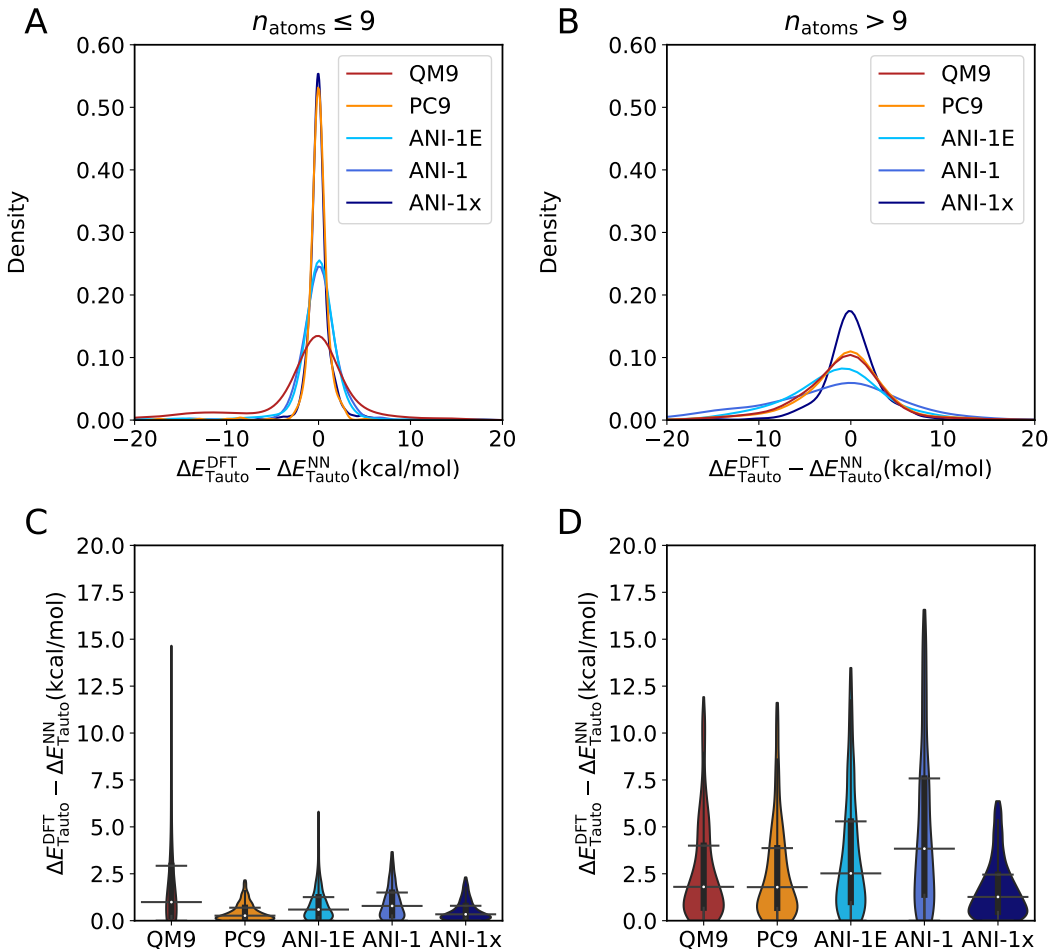


Figure 4: Error analysis on the prediction of the tautomerization energies. Panels A and B: Kernel density estimate of the error on the prediction of the tautomerization energies for the different databases evaluated in this work. Panels C and D: Normalized error distribution up to the 95% quantile of the different datasets for the errors in the tautomerization energy. The blackbox inside spans between the 25% and 75% quantiles with a white dot indicating the mean of the distribution. The whiskers indicate the 5% and 95% quantiles. The panels on the left and right are for Set1 and Set2, respectively.

In all cases studied, the distribution of errors for $\Delta \Delta E_{\text{Tauto}} = \Delta E_{\text{Tauto}}^{\text{DFT}} - \Delta E_{\text{Tauto}}^{\text{NN}}$ is centered around

zero. The width of the distribution depends on the reference dataset and on the number of atoms in the molecule. For Set1 (Figure 4A), the error distributions for PC9 and ANI-1x suggest high probabilities ($p(\Delta\Delta E_{\text{Tauto}}) = p(\Delta E_{\text{Tauto}}^{\text{DFT}} - \Delta E_{\text{Tauto}}^{\text{NN}})$), around 60 %, to obtain a small error. Conversely, QM9 performs worst with a maximum height of only $p(\Delta\Delta E_{\text{Tauto}}) \sim 15$ % and a faint maximum below $\Delta\Delta E_{\text{Tauto}} = -10$ kcal/mol to predict such energy differences with a larger probability than a positive value. The error distributions for ANI-1E and ANI-1 are similar in shape which indicates that their performance is comparable although the number of structures in ANI-1E is one order of magnitude smaller than that in ANI-1. Hence, adding additional structures (ANI-1 vs. ANI-1E) does not necessarily improve performance.

On the other hand, for Set2 (Figure 4B), the performance of QM9 and PC9 is comparable given the similar shape of their distribution of $p(\Delta\Delta E_{\text{Tauto}})$, ANI-1x gives the best predictions with a maximum height of around 15 % to obtain an error for ΔE_{Tauto} close to zero. All other reference data sets perform inferior with ANI-1 reaching only a 5 % $p(\Delta\Delta E_{\text{Tauto}})$ for a prediction close to zero. In addition, for most of the data sets the error distribution is asymmetric with an increased probability to predict a negative value for $\Delta\Delta E_{\text{Tauto}}$ compared to a positive value.

Results for the normalized error distributions $p(\Delta\Delta E_{\text{Tauto}})$ are shown in Figures 4C and D. For Set1, PC9 and ANI-1x show the smallest outliers by magnitude with an error below 2.5 kcal/mol. On the other hand, QM9 has the largest outliers with some errors larger than 15 kcal/mol. The average error for all reference distributions is around or below 1 kcal/mol for the 75 % quantile. For molecules in Set2, ANI-1 has the largest outliers, followed by ANI-1E, QM9, PC9, and ANI-1x performing best with a maximum error of around 5 kcal/mol, see Figure 4D.

For completeness, error distributions $p(\Delta E_{\text{SI}}) = p(E_{\text{SI}}^{\text{DFT}} - E_{\text{SI}}^{\text{NN}})$ for individual molecules and their normalized variants are also reported in Figures ??A to D. For Set1, the distributions for PC9 and ANI-1x are centered around zero with peak heights at 80 % which decreases to 25 % for ANI-

1E. For ANI-1 it is shifted to negative and for QM9 to positive values. For Set2 (Figure ??B), all error distributions are asymmetric and extend to large negative values of ΔE_{SI} . The best and worst performing reference distributions are ANI-1x and ANI-1, respectively. The normalized error distributions (Figures ??C and D) for both sets are strongly peaked. For Set1 (Figure ??C) the maxima for PC9 (2.5 kcal/mol) is the lowest whereas ANI-1 has the largest errors. For Set2 (Figure ??D), the outliers are even more pronounced with $|\Delta E_{SI}| > 100$ kcal/mol for ANI-1E and ANI-1. In general, the performance of ANI-1E is better than that of ANI-1 with a smaller MAE, outliers of smaller magnitude and a more compact distribution. These results are surprising, given the large difference between the size of both datasets (ANI-1E ($\approx 57k$) and ANI-1 ($\approx 20M$)) and confirm the earlier observation that addition of new structures to a database does not necessarily improve performance.

In summary, for Set1 the database with broader chemical diversity (PC9) and the database with the widest sampling of chemical and conformational space (ANI-1x) perform best. Hence, chemical diversity is essential for faithful prediction of ΔE_{Tauto} but it can be substituted to some extent with adequate sampling of conformational space. For larger molecules (Set2), the best results are obtained by ANI-1x which suggests that sampling of conformational space improves extrapolation to larger molecules. Datasets containing only equilibrium structures perform similarly for predicting ΔE_{Tauto} .

4 Effect of different database characteristics on predictions

This section analyzes the predictive power of the NNs trained on the five different training databases for tautomerization energies by considering various chemical properties such as the number of heavy atoms, the number of atoms of a given element, or the type of chemical bonds. Given the non-linear nature of the NN, the relationships between these characteristics and whether/how they

are related to the performance of the model is a challenging task. The features studied here were selected because they might be considered for the selection of a training database for the prediction of a chemical property (in this case the tautomerization energy) or because they can be optimized for the generation/enhancement of datasets used to train models for specific purposes.

4.1 Number of atoms

The first characteristic considered was the number of heavy atoms (C, N and O) contained in the reference data sets and how this affects the prediction quality on Tautobase. For Set1 the MAE for ΔE_{Tauto} typically decreases with increasing molecular size, see Figure 5A, for all five reference data sets. This can be broadly related to the increase in the number of molecules with the number of heavy atoms contained in the reference databases used for training (see Figure ??). For all data sets except for QM9, the MAE decreases to levels below 0.5 kcal/mol as the number of heavy atoms increases.

For larger molecules (Set2) in the Tautobase, the MAEs increase significantly, see Figure 5B. Broadly speaking, for up to 25 heavy atoms the MAE is still within 5 kcal/mol but increases considerably for larger molecules. ANI-1x performs best with MAE < 1 kcal/mol up to $n_{\text{atoms}} = 25$ but errors increase above 10 kcal/mol beyond that. This is followed by QM9 and PC9 which, on average, have MAEs of ~ 2 kcal/mol followed by ANI-1E and ANI-1.

The MAE for predicting E_{SI} for Set1 (Figure ??A) shows a slightly different profile than for ΔE_{Tauto} in that databases containing only equilibrium structures show large errors for molecules with 3 and 4 heavy atoms. With increasing size the error decreases. This is most pronounced for PC9 which eventually achieves the same quality as ANI-1x. It should be noted that for E_{SI} the overall shape of the profile of MAE vs. n_{atoms} for databases which only contain equilibrium structures is similar but the magnitude of the MAE differs. This is a consequence of the chemical diversity of the databases

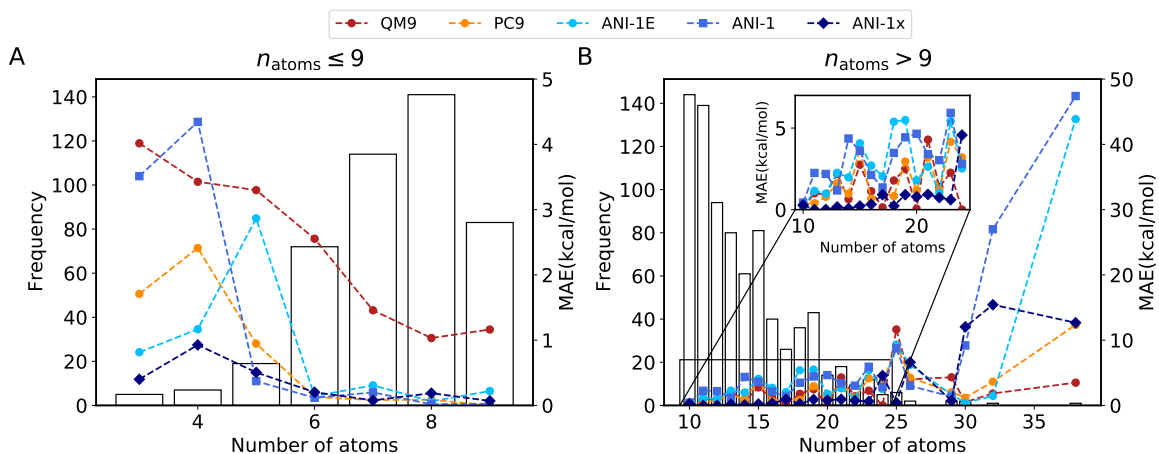


Figure 5: Mean Absolute Error (MAE) by number of heavy atoms (C,O,N) on the molecule for the tautomerization energy. The number of molecules for increasing number of heavy atoms is shown as a histogram. Panel A: Results for Set1, i.e. molecules with $n_{\text{atoms}} \leq 9$. Panel B: for Set2. The inset in panel B shows the MAE for ΔE_{Tauto} for $10 \leq n_{\text{atoms}} \leq 25$.

as discussed in subsection 4.4. For ANI-1 and Set1, the MAE is smallest for $n_{\text{atoms}} = 5$ and then starts to grow again. For Set2 (Figure ??B), the MAE displays a steady increase with the number of heavy atoms.

In summary, ANI-1x performs best across all values of n_{atoms} for the Tautobase, followed by PC9 across most values for n_{atoms} . For Set2, QM9 is quite reliable whereas ANI-1 and ANI-1E perform worst which reiterates the earlier finding that adding perturbed structures to a data set does not necessarily improve the quality on the task at hand (which is the estimation of ΔE_{Tauto}). Consequently, the results can be worse than those obtained when training only on equilibrium structures.

A further refinement can be made by analyzing the predictions for ΔE_{Tauto} in terms of the number of C-, N-, and O-atoms contained in the molecules of the reference database (Tautobase), see Figure 6. For Set1 the prediction error tends to decrease (except for QM9) with increasing number of carbon atoms as shown in Figure 6A whereas for Set2 it increases to different extents depending on the reference database considered, see Figure 6B. For nitrogen and oxygen atoms and ANI-1x all MAEs for Set1 and Set2 are small (~ 1 kcal/mol), except for the largest numbers of N-atoms,

see Figure 6F. For the PC9, ANI-1E, and ANI-1 databases and Set1 all MAEs are below or around 1 kcal/mol whereas for QM9 they can be larger. For Set2, the MAEs are up to 5 kcal/mol for molecules for which at least tens of representatives are contained in Tautobase, but start to increase significantly below that, see Figure 6D and F.

Considering the MAE for E_{SI} confirms these general findings, see Figure ???. For C-atoms the MAE for all reference databases decreases for Set1 except for $n_{\text{atoms}} = 8$ for ANI-1E and ANI-1, and increases moderately for Set2 with increasing value of n_{atoms} for QM9 and ANI-1x and more steeply for PC9, ANI-1E and ANI-1 (see Figures ??A and B). For nitrogen and oxygen atoms satisfactory performance is only found for PC9, ANI-1x and ANI-1E (Set1) and for QM9 and ANI-1x (Set2), see Figures ??C to F. Molecules with a small number of atoms of a given element have a reduced number of different chemical environments (see Figure ??). This makes it more difficult to predict ΔE_{Tauto} if that chemical environment is present in the target data set (Tautobase) but not sampled in the reference sets. Consequently, larger errors are observed for molecules with few atoms of a given element.

4.2 Structural composition of the chemical databases

The structural diversity of the databases can also be quantified in terms of the bond types that are covered. It can be assumed that the NN model learns that specific composition, and consequently, if the database used for training a NN model covers a large range of bond lengths, better results are expected. In the following, bond length distributions in the reference databases of equilibrium structures (PC9, QM9, and ANI-1E) are compared with the distributions contained in Tautobase. Figures ?? to ?? show that the reference and target distributions have a different coverage of bond lengths. The general finding is that for Set1 the overlap between reference and target distributions is better than for Set2.

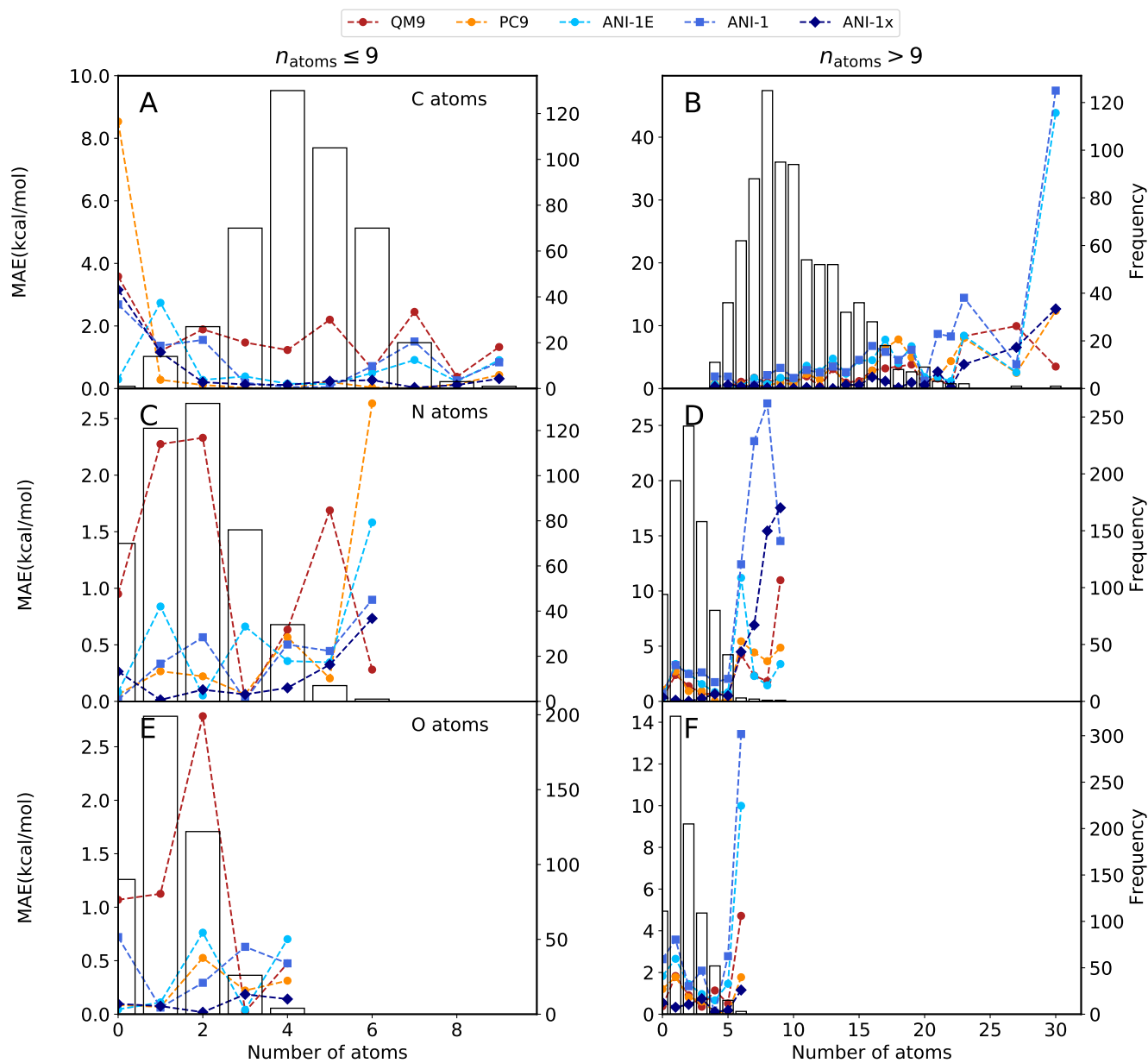


Figure 6: Mean Absolute Error (MAE) by number of atoms of a given element for the tautomerization energy. A histogram of the number of molecules for different numbers of heavy atoms is shown in the background. Panels A and B show the results by number of carbon atoms. Panels C and D shows the results by number of nitrogen atoms. Finally, panels E and F show the results by number of oxygen atoms. Left panel shows results for molecules with $n_{\text{atoms}} \leq 9$ the right for molecules with $n_{\text{atoms}} > 9$.

Figure ?? shows that C-C single bonds between $\text{C}(\text{sp}^3)$ atoms are well covered for the three reference databases compared with Tautobase. The $\text{C}(\text{sp}^2)\text{-C}(\text{sp}^2)$ double bonds are covered differently for the reference datasets: QM9 has the fewest examples of this type of bond, whereas ANI-1E

shows the best coverage. Such bonds are important for large molecules ($n_{\text{atoms}} > 9$) because of the presence of aromatic rings (Figure ??). Double C(sp²)-C(sp²) bonds close to hetero atoms are poorly covered by all reference datasets. Those bonds are crucial because they are the main origin of tautomerization rearrangement.

C(sp²)-N double bonds (Figure ??) are abundantly present in the Tautobase. However, the coverage of the reference datasets of that type of bond is heterogeneous; ANI-1E shows the best coverage followed by PC9 and QM9. On the other hand, C(sp²)-N bonds close to a heteroatom, more prevalent in larger molecules, are better covered by QM9 than PC9 whereas C(sp)-N bonds are well covered by all three databases. Carbon-Oxygen bonds for carbonyl groups are more predominant in Set1 and are well covered for the reference databases. Bonds for enols, esters and others are important for the Tautobase; PC9 covers such C-O bonds sufficiently but it is poorly sampled for QM9. Lastly, while C-O bonds of the type of alcohols and dialkyl ethers are most sampled for the reference databases they are least important for the Tautobase.

A quantitative measure for the overlap of two distributions is the KL divergence $D(p||q)$, see Equation 2. If the two distributions are identical, $D(p||q) = 0$. On the other hand, if the reference database $p(x)$ (here QM9, PC9, ANI-1E) contains more information than the target set $q(x)$ (Tautobase), $D(p||q) > 0$, and if specific information is missing, $D(p||q) < 0$. Hence, the cases for which $D(p||q) < 0$ are of particular relevance if improvements of the reference databases are sought for better capturing ΔE_{Tauto} .

The KL divergence analysis indicates that the coverage of the reference sets is heterogeneous, see Tables ??, ?? and Figure 7. There are several types of C-C bonds that are insufficiently covered, such as C(sp²)-C(sp²) single and double bonds, or C(ar)-C(ar) bonds. Also, certain types of C-N bonds would require more data as the bonds involving C(sp³) and C(sp²) with different types of nitrogens. Coverage of C-O bonds by the reference databases displays a bias toward al-

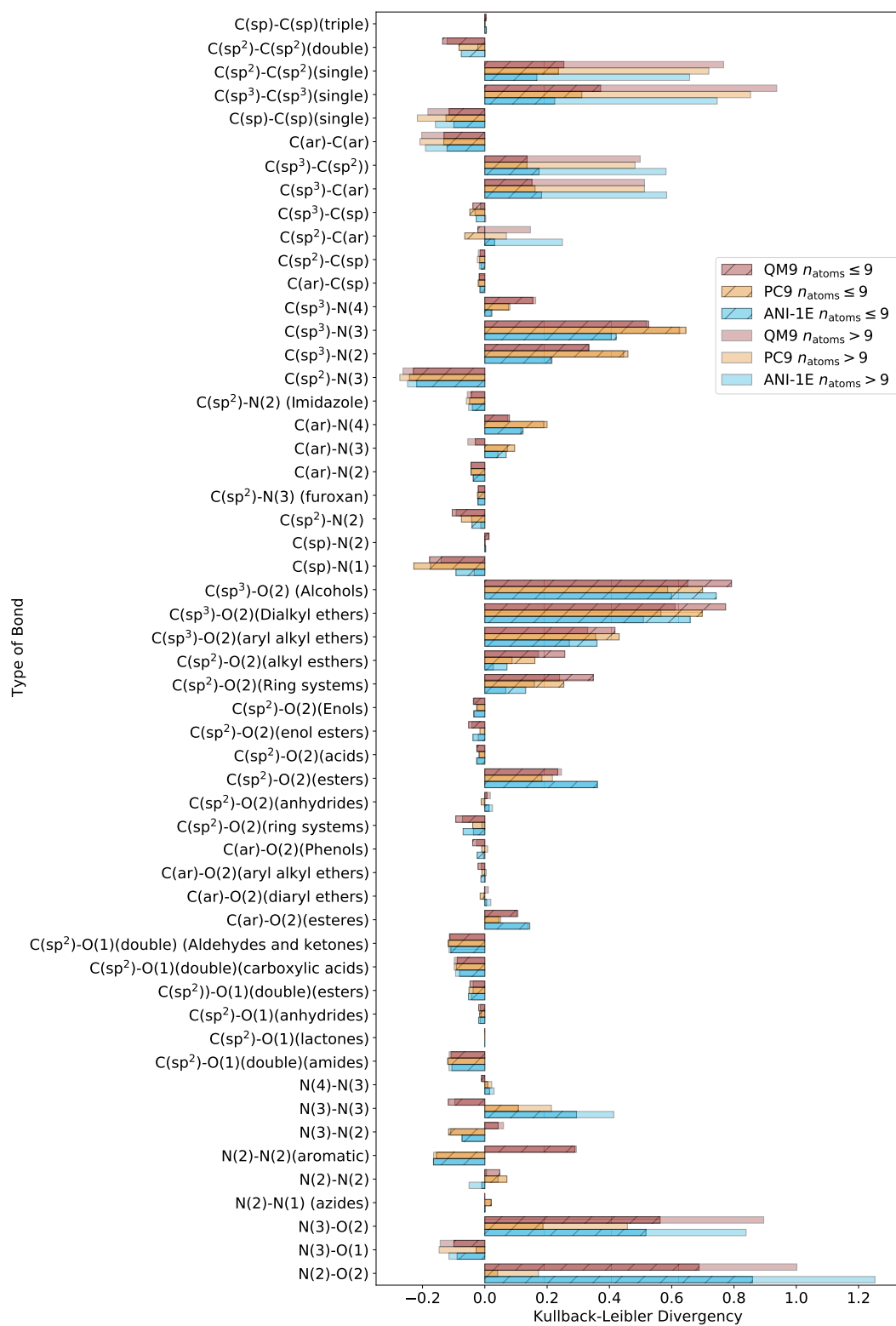


Figure 7: Values of the Kullback-Leibler divergence for different types of bonds present in the reference databases (QM9,PC9 and ANI-1E) compared with tautobase.

cohols, ethers and esters. Finally, N-N are the types of bond that show a more diverse coverage between databases, with some cases for which QM9 has a good coverage (N(3)-N(2) and N(2)-N(2)(aromatic)) but a poor coverage for N(3)-N(3). Interestingly, there are cases for which QM9 has a good coverage, whereas ANI-1E and PC9 are deficient. Figure 7 shows that none of the reference databases covers all of the predominant types of bonds present in the tautobase.

Next, the MAE for a specific number of a particular type of bond (e.g. C-C, C-O, or C-N) was determined for single isomer energies, see Figure 8. The results in Figure 8A show that for C-C bonds and Set1 the error for PC9 (orange) and ANI-1x (black) is constant and well below 1 kcal/mol. On the other hand, for QM9 (red) the error oscillates without following a clear trend. ANI-1E (light blue) and ANI-1 (dark blue) behave similarly to one another with a smaller MAE for ANI-1E than the one for ANI-1.

For C-O bonds, the MAE of the prediction of E_{SI} slowly increases for PC9 but remains well below 1 kcal/mol, whereas for QM9 it starts at above 5 kcal/mol and decreases to below 1 kcal/mol but always remaining above that for PC9, see Figure 8C. The error for the database of the ANI family is largely constant over the number of bonds. For ANI-1 the MAE oscillates between 1 kcal/mol and 2 kcal/mol, whereas for ANI-1E and ANI-1x the MAE is well below 1 kcal/mol, except for zero C-O bonds and ANI-1E. Considering C-N bonds (Figure 8E) it is found that their maximum number is larger than that for C-O bonds. The magnitude for the MAE for this bond type is at least a factor of three larger than that for the C-C and C-O bonds, respectively. Again, PC9 and ANI-1x perform best, followed by ANI-1E (except for molecules with only one C-N bond). The MAE for QM9 slowly decreases whereas that for ANI-1 is constant at below 2 kcal/mol up to five C-N bonds after which it sharply increases.

Regarding C-O and C-N bonds, it is clear that the good coverage of ANI-1E helps to reach small MAE when the number of bonds increases (Figure ??). These results show that PC9 has a

good overall performance because there is an adequate coverage of different chemical bond types whereas QM9 and ANI-1E have biases toward some types of bonds (Table ?? and ??). It should be stressed though that such an analysis excludes the fact that the same type of bond can behave differently given different chemical environments.

For Set2 the increase of the error with decreasing number of samples is more apparent. As discussed before, the MAE observed for larger molecules ($n_{\text{atoms}} > 9$) grows proportional with the number of bonds (See Figure 8 B, D and F). In this regard, ANI-1 and ANI-1E are the databases with largest growth rate, followed by PC9 and finally QM9 and ANI-1x. The low MAE for E_{SI} by number of bonds obtained with ANI-1x is a consequence of the addition of an adequate number of non-equilibrium structures. This suggests that a lack of chemical diversity can be partially compensated by including non-equilibrium structures in a database.

4.3 Initial Geometry

In the previous sections, the energy of the molecules was computed using the equilibrium geometry of the tautomeric pairs computed at the level of theory of the various reference databases used for training the NNs. However, in practice, it would be of interest to sidestep the computationally rather expensive optimization of the structures in the reference dataset (here Tautobase) at the density functional or even higher level of quantum chemical theory. For this, using empirical force fields is a possibility. A recent study for 3271 small organic molecules ($n_{\text{atoms}} < 50$), similar to those contained in Tautobase, found typical RMSDs of 0.25 Å to 1 Å between optimized structures at the B3LYP/6-31G* level of theory compared with those optimized by nine different force fields, including GAFF, MMFF94, OPLS and others.⁷³ Considering this, it is interesting to assess the performance of the NN-based models on FF-optimized geometries.

For this analysis, the geometries for molecules from Tautobase were optimized as described in

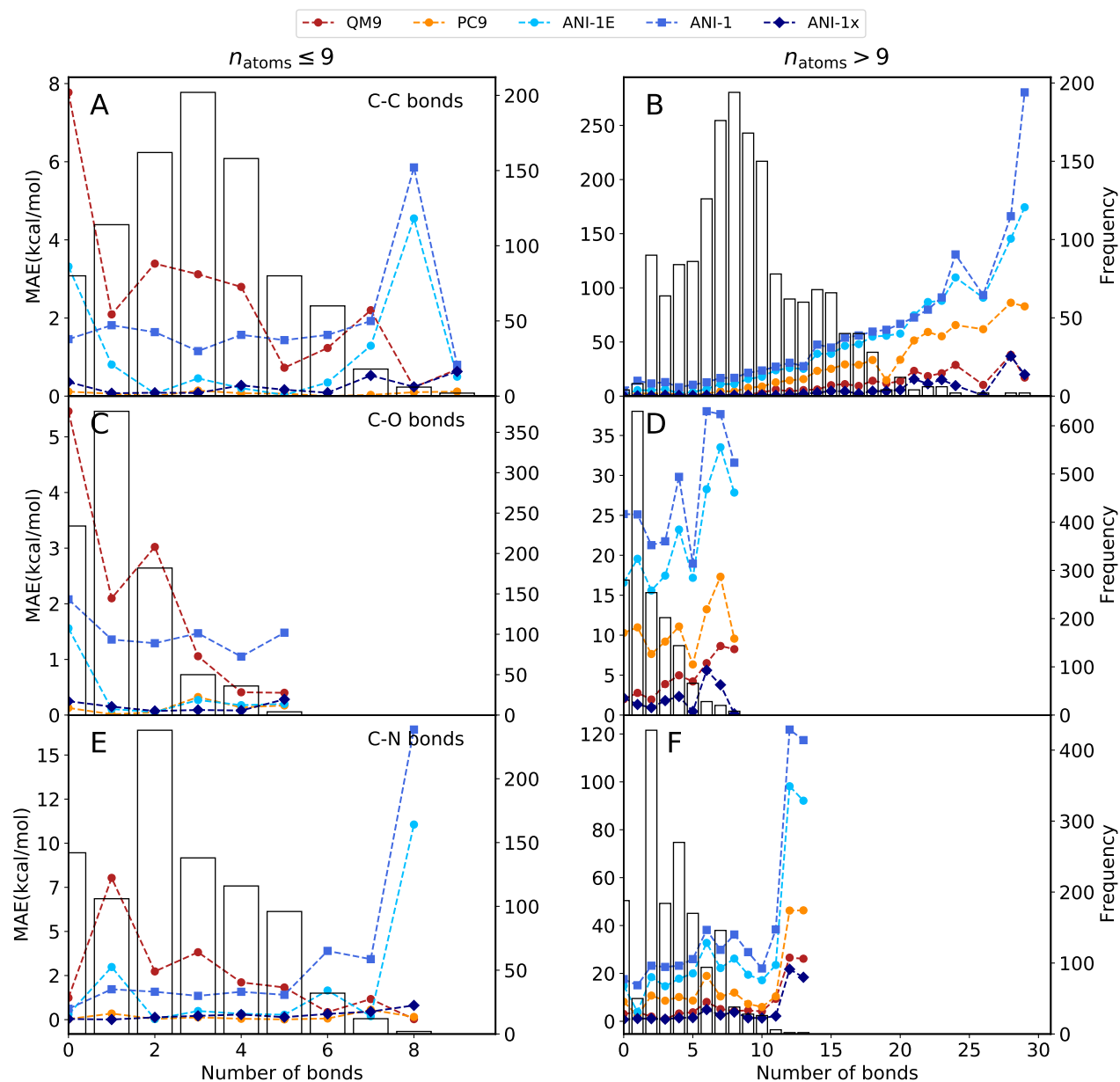


Figure 8: Mean Absolute Error (MAE) of the prediction of the energy of single isomers by number of bonds involving carbon atoms. The number of molecules for different numbers of bonds is shown as a histogram. Panels A and B correspond to the results of C-C bonds, panels C and D show the results for C-O bonds and panels E and F show the results for C-N bonds. Left panel for Set1 and right panel for Set2.

section 2.3 with the MMFF94 force field and then used to evaluate the tautomerization energies using the five trained NNs. Table ?? shows that the MAE for the tautomerization and single isomer energy increases for all evaluated models when the geometry used to evaluate the energies

differs from geometries optimized with the respective *ab initio* method. In all cases the MAE for ΔE_{Tauto} increases by a factor between 1.5 and 3 compared with the error obtained using the optimized geometries at the quantum chemical level of theory used to train the NN (see Table 2). A similar effect is observed for E_{SI} . It is noticeable that this geometry effect is less pronounced for databases which contain non-equilibrium structures: ANI-1 shows the smallest increase of the MAE for ΔE_{Tauto} compared with results from using optimized geometries at the appropriate level of theory.

Normalized distributions for ΔE_{Tauto} using MMFF94 geometries for Set1 (Figure ??C) indicate that the datasets which only cover chemical space (QM9, PC9 and ANI-1E) perform similarly with the highest values of the outliers close to 15 kcal/mol. Conversely, the other two databases (ANI-1 and ANI-1x) have a more compact distribution with the maximum values for outliers around 10 kcal/mol. Figure ??D shows that the most challenging case for predicting tautomerization energies is for Set2 with geometries generated with MMFF94. However, the performance is similar for all the datasets evaluated with outliers larger than 20 kcal/mol, except for ANI-1x with a maximum of 10 kcal/mol. These results demonstrate that the initial geometry passed to the NN model is essential for obtaining meaningful results. Scoring a model trained on minimum energy structures computed at a given level of quantum chemical theory can not be done using optimized structures from an empirical force field (or from structures at a sufficiently different level of quantum chemical theory).

To confirm this finding, a third set of molecules was evaluated using geometries generated by six popular force fields as described in Section 2. In the SAMPL2 challenge,⁶¹ the RMSD to DFT optimized geometries of several molecules were evaluated with respect to geometries obtained from various force fields. The energy predictions for the molecules on the SAMPL2 challenge (Figure ??) show no correlation between the geometry and the energy predicted by the NN. There are molecules with a small RMSD (e.g. $\leq 0.1 \text{ \AA}$) which display a significant error ($> 5 \text{ kcal/mol}$) in

predicting the energy by the NN models and vice versa. A possible explanation is that the change in geometry can be compensated by more extensive sampling of chemical space by the reference databases.

4.4 Visualization of chemical space

To understand the influence of the different databases studied on the performance of the models, it is of interest to analyze the coverage of ‘chemical space’. Firstly, molecules in the databases were deconstructed and their constituent amons (unique chemical fragments) were enumerated. PC9 contained the largest number of unique amons (8424), followed by QM9 (3929) and, finally, the ANI family of databases (1663). There is significant overlap of common amons between the datasets (Figure 9A, which suggests that they cover similar regions of chemical space. Regarding the overlap of the test set (Tautobase) with the databases tested, PC9 is the one which covers the most amons by number in the reference set, followed by ANI-1E and, QM9 (Figure 9B).

It is of interest to quantify the overlap of amons between the reference and target sets as done in figure 9. This provides a measure for the coverage of chemical space common to both sets and can be related to prediction errors for ΔE_{Tauto} . Comparing this overlap with the results obtained in 2, the database that covers the largest number of amons gives the smallest MAE for ΔE_{Tauto} . This is more evident if the MAEs for ΔE_{Tauto} for Set1 and Set2 are analyzed separately. For Set1, the results are consistent with the classification by number of amons (Figure 2 A, C and E). However, for Set2 the results of QM9 are better than those obtained with ANI-1E which contradicts the correlation with the number of amons in the databases (Figure 2 B, D and F). This can probably be explained by the fact that QM9 contains more large molecules which should help predicting the energy of single molecules accurately. This effect is also observed looking at the MAE for E_{SI} in Table 2 for which QM9 has a smaller MAE than PC9.

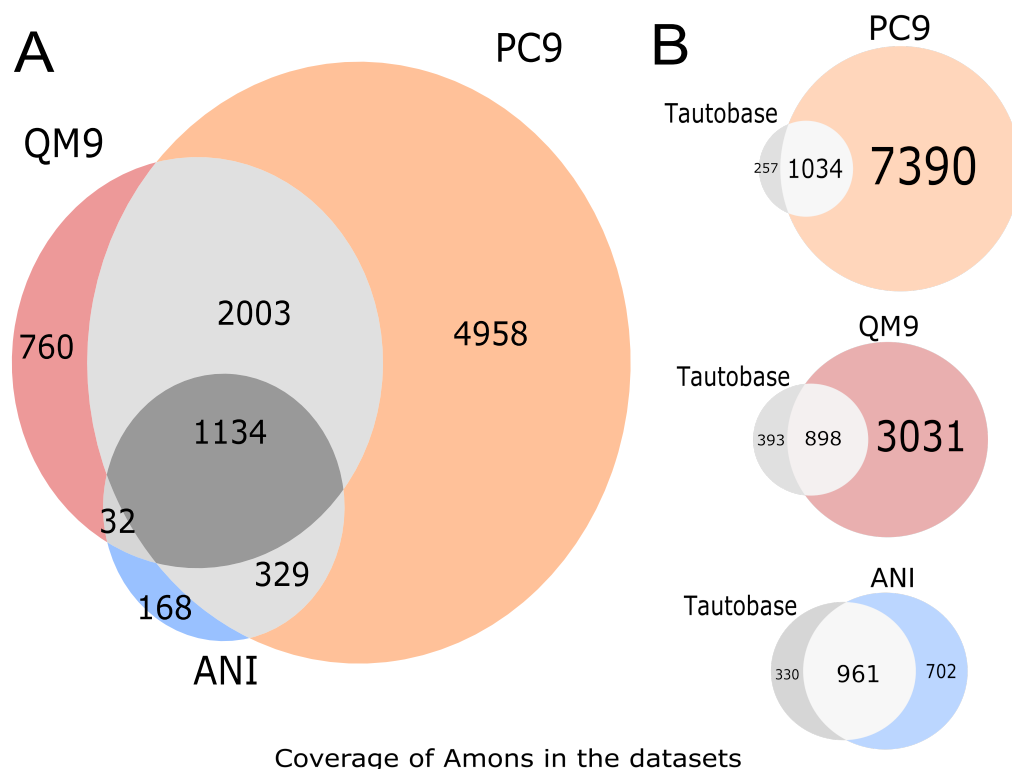


Figure 9: A) Venn diagram showing the overlap of amoms between the QM9,⁴⁹ PC9⁵⁰ and ANI⁵¹ family data sets. B) Overlap of amoms up to length five between three popular quantum chemistry datasets (QM9, PC9 and ANI-1E) and the ‘Tautobase’,⁴⁶ a collection of experimentally observed tautomers. Molecules containing other atoms than hydrogen, carbon, nitrogen, and oxygen were filtered from all datasets.

A more detailed analysis is possible by considering if the amoms of the isomers in the tautobase are present (or not) in the training databases. For this, a set ‘seen amoms’ (all constituent amoms included in the reference database) and ‘unseen amoms’ (molecules for which one or several amoms were missing from the reference set) was defined. The error distributions for both sets were determined and are reported in Figure 10. Perhaps unsurprisingly, the ‘seen amoms’ had a larger probability of obtaining a small error compared to the ‘unseen amoms’. Interestingly, PC9, which provides the broadest sampling of chemical space as quantified by the number of amoms in the database, showed a similar probability error distribution for Set1 and Set2. The errors for ‘unseen amoms’ using the NN trained on QM9, a significantly smaller dataset, shows a larger and more right-skewed distribution of errors. One possible explanation may be that a better exploration of

chemical space helps when predicting energies for molecules containing chemistry outside that covered by the database.

Regarding the ANI family of databases, the ANI-1 and ANI-1E results have similar error distributions. However, ANI-1x shows a smaller mean error for both the seen and unseen sets. These results are another indication that a random sampling of conformational space does not help improve the NN model predictions. On the contrary, it makes it worse than when only equilibrium structures are considered. Another notable finding is that ANI-1x shows similar performance for molecules with seen and unseen atoms. This can be explained given the good sampling of chemical space, which is the same as for ANI-1E, but combined with a broad exploration of conformational space by a refinement from ANI-1 using active learning.⁵⁷

Rational detection of systematic deficiencies in quantum chemical databases is challenging because of the high dimensionality of chemical space. For this reason, methods to visualise chemical space in a digestible way are highly desirable. A recent development is the TreeMAP (TMAP) algorithm, which allows for an interpretable, low dimensional representation of the test set's chemical space.⁷⁴ The TMAP algorithm constructs a weighted graph that is efficient for compact representations of high dimensional data. The necessary weights are based on the Jaccard distance, which measures the dissimilarity between the fingerprint of two structures. This graph is then pruned to the minimum spanning tree, a fully connected, acyclic sub-graph containing all nodes of the parent graph, and retaining only essential edges which minimize the weights. This organizes the compounds contained in a database into a tree, putting related structures on nearby branches. From this, groups of related moieties can be identified which are potentially detrimental to predicting the quantity in question, here ΔE_{Tauto} .

For instance, coloring the nodes of Tautobase TMAP by error of tautomerization energy (Figure 10F) reveals that structures with azoles containing N-N and N-O bonds correlate with large errors.

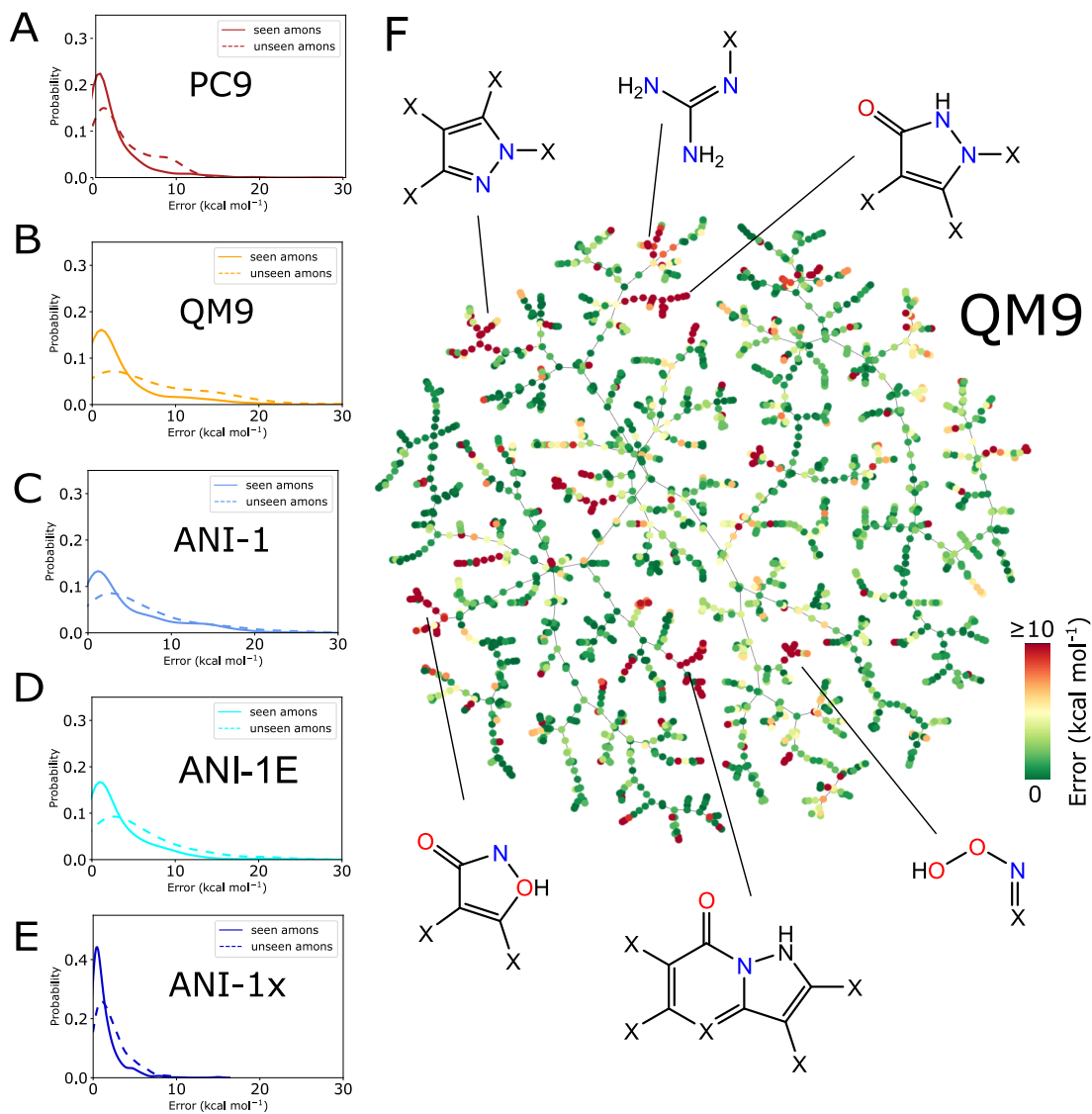


Figure 10: The relationship between chemical space and model reliability. Panels A to E: The mean average absolute error for molecules from Tautobase with one or more amons outside the training set is larger than if all amons are present, a trend observed for all databases. Panel F: Projection of the Tautobase using the TMAP algorithm identifies ‘branches’ of chemical space that are poorly predicted by the neural network models. The error displayed here is for the QM9 database. TMAPs for all databases used for training are available as interactive plots which can be viewed in a web browser, which can be obtained in the supporting information.

Interestingly, KL-divergences for these types of bond distances suggested that they were under-represented in the reference sets, see Figure 7. The moieties corresponding to large errors change based on the different databases used to train the NN model, see Figure ???. Interactive plots are available in the supporting information.

5 Discussion and Conclusions

The prominence of ML has raised concerns regarding the 'interpretability' of the models conceived.^{24,75} This awareness also increases for complex models because a rational relationship between initial data used for training and resulting prediction becomes less transparent. Therefore, it is important to develop quantifiable and intuitive tests for how ML models "work" and how trustworthy predictions by them are.⁷⁶ One recently proposed procedure is "post-hoc" interpretation for which the practitioner analyzes a trained model with the aim to understand what the model has learned from the data without changing the underlying model.^{21,23} In this work, post-hoc interpretability techniques were used to investigate the effect of different features of the database on predicting a chemical property (tautomerization energy). The selected features are considered important for the construction of robust quantum chemical databases for ML. In the present case this implied the analysis of individual features of several databases to quantify how these modify the prediction of a chemical property on an unseen set of examples using statistics and visualization techniques. With sufficient information from such an analysis it is expected that it will be possible to identify which features of the training databases are essential for good performance on a given task, making a rational design/enhancement of databases for training ML models for a given task possible.

The present work aimed at quantifying and analyzing the suitability of NNs trained on five different reference data sets (QM9, PC9, ANI-1E, ANI-1, and ANI-1x) to predict the tautomerization energies of molecules contained in Tautobase. It was found that depending on which characteristics are considered, the predicted MAEs can behave very differently and can, in part, be related to geometrical and/or chemical properties encoded in the databases. Such analyses attempt to digress from "black box" applications of ML methods and move towards "interpretable ML". Hence, one

of the questions is “what features need to be present and covered in a training database for application to a concrete chemical question”. In the present case the databases to choose from were QM9, PC9, ANI-1E, ANI-1, and ANI-1x’ and the application was computation of the gas phase tautomerization energy.

The results indicate that the exploration of chemical space is essential for meaningful results. The coverage of chemical space can be quantified by the chemical diversity expressed as the number of amons on the database (see Figure 9). The energy prediction improves when the overlap of the number of amons in the training set and the tautobase increases. If the number of amons in the chemical database does not cover all the amons on the target set, addition of non-equilibrium structures to the training set can improve the results. That addition needs to be done following a rational strategy because an arbitrary addition causes deficiencies in the model, leading to poor results as seen for the results for ANI-1E and ANI-1.

Another determinant property is the number of heavy atoms in molecules covered in the database. Not surprisingly, better results are obtained for the range covered by the database. Outside that range, the energy prediction quality decreases with the number of atoms for most databases. One of the training databases (ANI-1x) shows good results because the non-equilibrium structures help in predicting the energies. It was observed that the different chemical environments need to be thoroughly sampled because functional diversity is key to assure good results.

The structural composition of the data sets used for training the NNs (QM9, PC9 and ANI-1E) and the data set to which the trained models were applied to (Tautobase) can be compared through the Kullback-Leibler divergence. The overlap between these distributions already provides an indication how suitable a particular reference data set will be for application to the target task. In other words: the KL divergence can be used for the rational design of databases for NN models. It will be of interest to extend this to angles and dihedrals for a comprehensive exploration of the

structural overlap. The geometry of the molecule to evaluate the trained NN is essential for good performance. Using the TMAP algorithm it was possible to identify regions of chemical space that are poorly covered by the trained models. This is an excellent aid because it becomes easier to improve sampling of a specific region of chemical space to obtain better results. The characteristics of the databases analyzed in the present work can be used as a rational basis to determine whether a database is suitable for a specific prediction task.

In conclusion, the present work demonstrates that ML-trained models on five different reference databases and applied to one specific task (tautomerization energy) perform with a MAE ranging from 1.7 kcal/mol to 4.6 kcal/mol. The best performing reference database (ANI-1x with 5 M structures) performs on average by 1 kcal/mol better than PC9 which contains about two orders of magnitude fewer reference structures (≈ 85 K). On the other hand, PC9 is chemically more diverse by a factor of 5 (as judged from the number of amons) compared with the ANI family of databases. This indicates that lack in chemical diversity can be compensated for by increased number of non-equilibrium structures. However, the scaling of these two properties is very different. Together with quantitative descriptors, such as the KL divergence, the present results and analyses suggest that a rational approach to database generation for specific tasks may be possible.

Data Availability Statement

The PhysNet codes are available at Github (<https://github.com/MMunibas/PhysNet>) . The database for ANI-1E (10.5281/zenodo.4680953) and the geometries used for the tautobase (10.5281/zenodo.4680972) are available at Zenodo.

Acknowledgment

The authors acknowledge financial support from the Swiss National Science Foundation (NCCR-MUST and Grant No. 200021-7117810) and the University of Basel. OTU acknowledges funding from the Swiss National Science Foundation (Grant No. P2BSP2_188147).

References

- (1) Butler, K. T.; Davies, D. W.; Cartwright, H.; Isayev, O.; Walsh, A. Machine learning for molecular and materials science. *Nature* **2018**, *559*, 547–555.
- (2) Unke, O. T.; Chmiela, S.; Sauceda, H. E.; Gastegger, M.; Poltavsky, I.; Schütt, K. T.; Tkatchenko, A.; Müller, K.-R. Machine learning force fields. *Chem. Rev.* **2021 In Press**,
- (3) von Lilienfeld, O. A.; Burke, K. Retrospective on a decade of machine learning for chemical discovery. *Nat. Comm.* **2020**, *11*, 1–4.
- (4) Noé, F.; Tkatchenko, A.; Müller, K.-R.; Clementi, C. Machine learning for molecular simulation. *Annu. Rev. Phys. Chem.* **2020**, *71*, 361–390.
- (5) Agrawal, A.; Choudhary, A. Perspective: Materials informatics and big data: Realization of the “fourth paradigm” of science in materials science. *Apl Mater.* **2016**, *4*, 053208.
- (6) Aspuru-Guzik, A.; Lindh, R.; Reiher, M. The matter simulation (r) evolution. *ACS Cent. Sci.* **2018**, *4*, 144–152.
- (7) Behler, J.; Parrinello, M. Generalized neural-network representation of high-dimensional potential-energy surfaces. *Phys. Rev. Lett.* **2007**, *98*, 146401.
- (8) Bartók, A. P.; Payne, M. C.; Kondor, R.; Csányi, G. Gaussian approximation potentials: The accuracy of quantum mechanics, without the electrons. *Phys. Rev. Lett.* **2010**, *104*, 136403.
- (9) Rupp, M.; Tkatchenko, A.; Müller, K.-R.; Von Lilienfeld, O. A. Fast and accurate modeling of molecular atomization energies with machine learning. *Phys. Rev. Lett.* **2012**, *108*, 058301.
- (10) Montavon, G.; Rupp, M.; Gobre, V.; Vazquez-Mayagoitia, A.; Hansen, K.; Tkatchenko, A.; Müller, K.-R.; Von Lilienfeld, O. A. Machine learning of molecular electronic properties in chemical compound space. *New J. Phys.* **2013**, *15*, 095003.

- (11) Faber, F. A.; Hutchison, L.; Huang, B.; Gilmer, J.; Schoenholz, S. S.; Dahl, G. E.; Vinyals, O.; Kearnes, S.; Riley, P. F.; Von Lilienfeld, O. A. Prediction errors of molecular machine learning models lower than hybrid DFT error. *J. Chem. Theory Comput.* **2017**, *13*, 5255–5264.
- (12) Schütt, K. T.; Sauceda, H. E.; Kindermans, P.-J.; Tkatchenko, A.; Müller, K.-R. SchNet—A deep learning architecture for molecules and materials. *J. Chem. Phys.* **2018**, *148*, 241722.
- (13) Unke, O. T.; Meuwly, M. A reactive, scalable, and transferable model for molecular energies from a neural network approach based on local information. *J. Chem. Phys.* **2018**, *148*, 241708.
- (14) Wilkins, D. M.; Grisafi, A.; Yang, Y.; Lao, K. U.; DiStasio, R. A.; Ceriotti, M. Accurate molecular polarizabilities with coupled cluster theory and machine learning. *Proc. Natl. Acad. Sci. USA* **2019**, *116*, 3401–3406.
- (15) Veit, M.; Wilkins, D. M.; Yang, Y.; DiStasio Jr, R. A.; Ceriotti, M. Predicting molecular dipole moments by combining atomic partial charges and atomic dipoles. *J. Chem. Phys.* **2020**, *153*, 024113.
- (16) Unke, O. T.; Koner, D.; Patra, S.; Käser, S.; Meuwly, M. High-dimensional potential energy surfaces for molecular simulations: from empiricism to machine learning. *Mach. Learn.: Sci. Technol.* **2020**, *1*, 013001.
- (17) Ko, T. W.; Finkler, J. A.; Goedecker, S.; Behler, J. A fourth-generation high-dimensional neural network potential with accurate electrostatics including non-local charge transfer. *Nat. Comm.* **2021**, *12*, 1–11.
- (18) Von Lilienfeld, O. A. Quantum machine learning in chemical compound space. *Angew. Chem. Int. Ed.* **2018**, *57*, 4164–4169.
- (19) Heinen, S.; Schwilk, M.; von Rudorff, G. F.; von Lilienfeld, O. A. Machine learning the computational cost of quantum chemistry. *Mach. Learn.: Sci. Technol.* **2020**, *1*, 025002.

- (20) Käser, S.; Koner, D.; Christensen, A. S.; von Lilienfeld, O. A.; Meuwly, M. Machine Learning Models of Vibrating H₂CO: Comparing Reproducing Kernels, FCHL, and PhysNet. *J. Phys. Chem. A* **2020**, *124*, 8853–8865.
- (21) Du, M.; Liu, N.; Hu, X. Techniques for interpretable machine learning. *Commun. ACM* **2019**, *63*, 68–77.
- (22) Samek, W.; Müller, K.-R. *Explainable AI: interpreting, explaining and visualizing deep learning*; Springer, 2019; pp 5–22.
- (23) Murdoch, W. J.; Singh, C.; Kumbier, K.; Abbasi-Asl, R.; Yu, B. Definitions, methods, and applications in interpretable machine learning. *Proc. Natl. Acad. Sci. USA* **2019**, *116*, 22071–22080.
- (24) Dybowski, R. Interpretable machine learning as a tool for scientific discovery in chemistry. *New J Chem* **2020**, *44*, 20914–20920.
- (25) Wilkinson, A.; McNaught, A. IUPAC Compendium of Chemical Terminology,(the" Gold Book"). *International Union of Pure and Applied Chemistry: Zürich, Switzerland* **1997**,
- (26) Raczyńska, E. D.; Kosińska, W.; Ośmiałowski, B.; Gawinecki, R. Tautomeric equilibria in relation to pi-electron delocalization. *Chem Rev* **2005**, *105*, 3561–3612.
- (27) Martin, Y. C. Let's not forget tautomers. *J. Comput. Aided Mol. Des.* **2009**, *23*, 693–704.
- (28) Watson, J. D.; Crick, F. H. Molecular structure of nucleic acids: a structure for deoxyribose nucleic acid. *Nature* **1953**, *171*, 737–738.
- (29) Shukla, M. K.; Leszczynski, J. Tautomerism in nucleic acid bases and base pairs: a brief overview. *Wires Comput. Mol Sci.* **2013**, *3*, 637–649.
- (30) Singh, V.; Fedeles, B. I.; Essigmann, J. M. Role of tautomerism in RNA biochemistry. *RNA* **2015**, *21*, 1–13.

- (31) Käser, S.; Unke, O. T.; Meuwly, M. Isomerization and decomposition reactions of acetaldehyde relevant to atmospheric processes from dynamics simulations on neural network-based potential energy surfaces. *J. Chem. Phys.* **2020**, *152*, 214304.
- (32) Sitzmann, M.; Ihlenfeldt, W.-D.; Nicklaus, M. C. Tautomerism in large databases. *J. Comput. Aided Mol. Des.* **2010**, *24*, 521–551.
- (33) Greenwood, J. R.; Calkins, D.; Sullivan, A. P.; Shelley, J. C. Towards the comprehensive, rapid, and accurate prediction of the favorable tautomeric states of drug-like molecules in aqueous solution. *J. Comput. Aided Mol. Des.* **2010**, *24*, 591–604.
- (34) Pospisil, P.; Ballmer, P.; Scapozza, L.; Folkers, G. Tautomerism in computer-aided drug design. *J. Recept. Signal Transduct.* **2003**, *23*, 361–371.
- (35) Taylor, P. J.; van der Zwan, G.; Antonov, L. Tautomerism: Introduction, history, and recent developments in experimental and theoretical methods. *Tautomerism: methods and theories* **2014**, 1–24.
- (36) Fogarasi, G. Studies on tautomerism: benchmark quantum chemical calculations on formamide and formamidine. *J. Mol. Struct.* **2010**, *978*, 257–262.
- (37) Käser, S.; Unke, O. T.; Meuwly, M. Reactive dynamics and spectroscopy of hydrogen transfer from neural network-based reactive potential energy surfaces. *New J. Phys.* **2020**, *22*, 055002.
- (38) Baughcum, S. L.; Duerst, R. W.; Rowe, W. F.; Smith, Z.; Wilson, E. B. Microwave Spectroscopic Study Of Malonaldehyde (3-Hydroxy-2-Prop enal) .2. Structure, Dipole-Moment, and Tunneling. *J. Am. Chem. Soc.* **1981**, *103*, 6296–6303.
- (39) Firth, D. W.; Beyer, K.; Dvorak, M. A.; Reeve, S. W.; Grushow, A.; Leopold, K. R. Tunable far infrared spectroscopy of malonaldehyde. *J. Chem. Phys.* **1991**, *94*, 1812–1819.

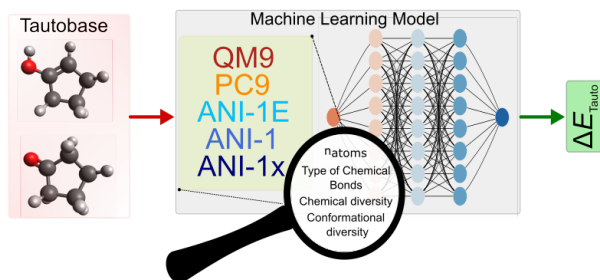
- (40) Limbach, H.-H.; Wehrle, B.; Zimmermann, H.; Kendrick, R. D.; Yannoni, C. S. Kinetic ¹⁵N-CPMAS-NMR Study of a Double Proton Transfer in a Crystalline Malonaldehyde Diimine Derivative. *Angew. Chem. Int. Ed.* **1987**, *26*, 247–248.
- (41) Wang, Y.; Braams, B. J.; Bowman, J. M.; Carter, S.; Tew, D. P. Full-dimensional quantum calculations of ground-state tunneling splitting of malonaldehyde using an accurate *ab initio* potential energy surface. *J. Chem. Phys.* **2008**, *128*, 224314.
- (42) Schröder, M.; Gatti, F.; Meyer, H.-D. Theoretical studies of the tunneling splitting of malonaldehyde using the multiconfiguration time-dependent Hartree approach. *J. Chem. Phys.* **2011**, *134*, 234307.
- (43) Yang, Y.; Meuwly, M. A generalized reactive force field for nonlinear hydrogen bonds: Hydrogen dynamics and transfer in malonaldehyde. *J. Chem. Phys.* **2010**, *133*, 064503.
- (44) Karandashev, K.; Xu, Z.-H.; Meuwly, M.; Vaníček, J.; Richardson, J. O. Kinetic isotope effects and how to describe them. *Struct. Dyn.* **2017**, *4*, 061501.
- (45) Unke, O. T.; Meuwly, M. PhysNet: a neural network for predicting energies, forces, dipole moments and partial charges. *J. Chem. Theory Comput.* **2019**, *15*, 3678–3693.
- (46) Wahl, O.; Sander, T. Tautobase: An Open Tautomer Database. *J. Chem. Inf. Model.* **2020**, *60*, 1085–1089.
- (47) Dhaked, D. K.; Guasch, L.; Nicklaus, M. C. Tautomer Database: A Comprehensive Resource for Tautomerism Analyses. *J. Chem. Inf. Model.* **2020**, *60*, 1090–1100.
- (48) Huang, B.; von Lilienfeld, O. A. Quantum machine learning using atom-in-molecule-based fragments selected on the fly. *Nat. Chem.* **2020**, 1–7.
- (49) Ramakrishnan, R.; Dral, P. O.; Rupp, M.; Von Lilienfeld, O. A. Quantum chemistry structures and properties of 134 kilo molecules. *Sci. Data* **2014**, *1*, 140022.

- (50) Glavatskikh, M.; Leguy, J.; Hunault, G.; Cauchy, T.; Da Mota, B. Dataset's chemical diversity limits the generalizability of machine learning predictions. *J. Cheminf.* **2019**, *11*, 69.
- (51) Smith, J. S.; Isayev, O.; Roitberg, A. E. ANI-1, A data set of 20 million calculated off-equilibrium conformations for organic molecules. *Sci. Data* **2017**, *4*, 3192–3203.
- (52) Smith, J. S.; Zubatyuk, R.; Nebgen, B.; Lubbers, N.; Barros, K.; Roitberg, A. E.; Isayev, O.; Tretiak, S. The ANI-1ccx and ANI-1x data sets, coupled-cluster and density functional theory properties for molecules. *Sci. Data* **2020**, *7*, 1–10.
- (53) Ruddigkeit, L.; Van Deursen, R.; Blum, L. C.; Reymond, J.-L. Enumeration of 166 billion organic small molecules in the chemical universe database GDB-17. *J. Chem. Inf. Model.* **2012**, *52*, 2864–2875.
- (54) Nakata, M.; Shimazaki, T. PubChemQC project: a large-scale first-principles electronic structure database for data-driven chemistry. *J. Chem. Inf. Model.* **2017**, *57*, 1300–1308.
- (55) Fink, T.; Bruggesser, H.; Reymond, J.-L. Virtual exploration of the small-molecule chemical universe below 160 daltons. *Angew. Chem. Int. Ed.* **2005**, *44*, 1504–1508.
- (56) Fink, T.; Reymond, J.-L. Virtual exploration of the chemical universe up to 11 atoms of C, N, O, F: assembly of 26.4 million structures (110.9 million stereoisomers) and analysis for new ring systems, stereochemistry, physicochemical properties, compound classes, and drug discovery. *J. Chem. Inf. Model.* **2007**, *47*, 342–353.
- (57) Smith, J. S.; Nebgen, B.; Lubbers, N.; Isayev, O.; Roitberg, A. E. Less is more: Sampling chemical space with active learning. *J. Chem. Phys.* **2018**, *148*, 241733.
- (58) Smith, J. S.; Isayev, O.; Roitberg, A. E. ANI-1: an extensible neural network potential with DFT accuracy at force field computational cost. *Chem. Sci.* **2017**, *8*, 3192–3203.
- (59) O'Boyle, N. M.; Banck, M.; James, C. A.; Morley, C.; Vandermeersch, T.; Hutchison, G. R. Open Babel: An open chemical toolbox. *J. Cheminf.* **2011**, *3*, 33.

- (60) Halgren, T. A. Merck molecular force field. I. Basis, form, scope, parameterization, and performance of MMFF94. *J. Comput. Chem.* **1996**, *17*, 490–519.
- (61) Geballe, M. T.; Skillman, A. G.; Nicholls, A.; Guthrie, J. P.; Taylor, P. J. The SAMPL2 blind prediction challenge: introduction and overview. *J. Comput. Aided Mol. Des.* **2010**, *24*, 259–279.
- (62) Foloppe, N.; MacKerell, A. D., Jr All-atom empirical force field for nucleic acids: I. Parameter optimization based on small molecule and condensed phase macromolecular target data. *J. Comput. Chem.* **2000**, *21*, 86–104.
- (63) Wang, J.; Wolf, R. M.; Caldwell, J. W.; Kollman, P. A.; Case, D. A. Development and testing of a general amber force field. *J. Comput. Chem.* **2004**, *25*, 1157–1174.
- (64) Jorgensen, W. L.; Tirado-Rives, J. The OPLS force field for proteins. Energy minimizations for crystals of cyclic peptides and crambin. *J. Am. Chem. Soc.* **1988**, *110*, 1657–1666.
- (65) Rappé, A. K.; Casewit, C. J.; Colwell, K.; Goddard III, W. A.; Skiff, W. M. UFF, a full periodic table force field for molecular mechanics and molecular dynamics simulations. *J. Am. Chem. Soc.* **1992**, *114*, 10024–10035.
- (66) Schmid, N.; Eichenberger, A. P.; Choutko, A.; Riniker, S.; Winger, M.; Mark, A. E.; van Gunsteren, W. F. Definition and testing of the GROMOS force-field versions 54A7 and 54B7. *Eur. Biophys. J.* **2011**, *40*, 843–856.
- (67) Hassinen, T.; Peräkylä, M. New energy terms for reduced protein models implemented in an off-lattice force field. *J. Comput. Chem.* **2001**, *22*, 1229–1242.
- (68) Stewart, J. J. Optimization of parameters for semiempirical methods VI: more modifications to the NDDO approximations and re-optimization of parameters. *J. Mol. Model.* **2013**, *19*, 1–32.

- (69) Stewart, J. J. MOPAC2016. *Stewart Computational Chemistry: Colorado Springs, CO, USA 2016*,
- (70) Frisch, M. J.; Trucks, G.; Schlegel, H.; Scuseria, G.; Robb, M.; Cheeseman, J.; Scalmani, G.; Barone, V.; Mennucci, B.; Petersson, G. et al. Gaussian 09, Revision D. 01, Gaussian. Inc.: Wallingford, CT **2009**,
- (71) Diwekar, U.; David, A. *BONUS Algorithm for Large Scale Stochastic Nonlinear Programming Problems*; Springer, 2015; pp 27–34.
- (72) Cover, T. M.; Thomas, J. A. *Elements of Information Theory*; Wiley Series in Telecommunications and Signal Processing; John Wiley & Sons, 2006.
- (73) Lim, V. T.; Hahn, D. F.; Tresadern, G.; Bayly, C. I.; Mobley, D. L. Benchmark assessment of molecular geometries and energies from small molecule force fields. *F1000Res.* **2020**, *9*, 1390.
- (74) Probst, D.; Reymond, J.-L. Visualization of very large high-dimensional data sets as minimum spanning trees. *J. Cheminf.* **2020**, *12*, 12.
- (75) Lipton, Z. C. The Mythos of Model Interpretability: In machine learning, the concept of interpretability is both important and slippery. *ACM Queue* **2018**, *16*, 31–57.
- (76) Schütt, K. T.; Gastegger, M.; Tkatchenko, A.; Müller, K.-R. *Explainable AI: Interpreting, Explaining and Visualizing Deep Learning*; Springer, 2019; pp 311–330.

Table of Content



Supporting Information: Impact of the characteristics of quantum chemical databases on machine learning predictions of tautomerization energies.

Luis Itza Vazquez-Salazar,[†] Eric Boittier,[†] Oliver T. Unke,^{‡,¶} and Markus Meuwly^{*,§,||}

[†]*Department of Chemistry, University of Basel, Klingelbergstrasse 80, CH-4056 Basel, Switzerland*

[‡]*Machine Learning Group, Technische Universität Berlin, 10587 Berlin, Germany*

[¶]*DFG Cluster of Excellence “Unifying Systems in Catalysis” (UniSysCat), Technische Universität Berlin, 10623 Berlin, Germany*

[§]*Department of Chemistry, University of Basel, Klingelbergstrasse 80, CH-4056 Basel, Switzerland.*

^{||}*Department of Chemistry, Brown University, Providence RI, USA*

E-mail: m.meuwly@unibas.ch

April 14, 2021

Supplementary Methods

Generation of the geometries for the molecules of the SAMPL2 challenge

The molecules of the SAMPL2 challenge[?] were used to generate a third database for the evaluation of the energies by the NN models containing only equilibrium molecules. The initial geometries generation was done using OpenBabel[?] for the force fields GAFF,[?] UFF[?] and Ghemical[?] for 5000 steps from the SMILES representations.

For the Gromos[?] force field, the parametrization of the molecules was done using the ATB server.[?] Meanwhile, the parameters for the CHARMM[?] force field were generated using Swiss-Param.[?] Finally, the parameters of the OPLS[?] force field were generated using the LigParGen[?] code. Once the parameters from those force fields were generated, the molecules were optimized for 5000 steps using the GROMACS code.

Table S1: Values of the Kullback-Leibler (KL) divergence of the different training sets and the tautobase at specific intervals for different types of bonds for molecules with $n_{\text{atoms}} \leq 9$. The values of the bond lengths were taken from Allen, F.H., *et al.*, 2006³

| Type of Bond | QM9 | PC9 | ANI-1E | Interval(Å) |
|-------------------------------------------------|---------|---------|---------|-------------|
| C(sp)-C(sp)(triple) | 0.003 | 0.000 | 0.005 | 1.167-1.197 |
| C(sp ²)-C(sp ²)(double) | -0.136 | -0.083 | -0.076 | 1.280-1.405 |
| C(sp ²)-C(sp ²)(single) | 0.254 | 0.236 | 0.167 | 1.400-1.568 |
| C(sp ³)-C(sp ³)(single) | 0.372 | 0.312 | 0.224 | 1.458-1.610 |
| C(sp)-C(sp)(single) | -0.114 | -0.125 | -0.099 | 1.374-1.474 |
| C(ar)-C(ar) | -0.131 | -0.132 | -0.121 | 1.350-1.440 |
| C(sp ³)-C(sp ²) | 0.136 | 0.135 | 0.174 | 1.470-1.538 |
| C(sp ³)-C(ar) | 0.151 | 0.161 | 0.182 | 1.479-1.539 |
| C(sp ³)-C(sp) | -0.038 | -0.048 | -0.027 | 1.436-1.481 |
| C(sp ²)-C(ar) | -0.022 | -0.065 | 0.031 | 1.441-1.512 |
| C(sp ²)-C(sp) | -0.015 | -0.016 | -0.013 | 1.425-1.441 |
| C(ar)-C(sp) | -0.017 | -0.019 | -0.015 | 1.430-1.448 |
| Carbon-Nitrogen bonds | | | | |
| C(sp ³)-N(4) | 0.1541 | 0.0765 | 0.0205 | 1.482-1.510 |
| C(sp ³)-N(3) | 0.5254 | 0.6454 | 0.4214 | 1.446-1.572 |
| C(sp ³)-N(2) | 0.3340 | 0.4596 | 0.2156 | 1.461-1.506 |
| C(sp ²)-N(3) | -0.2290 | -0.2421 | -0.2186 | 1.314-1.419 |
| C(sp ²)-N(2) (Imidazole) | -0.0432 | -0.0488 | -0.0402 | 1.369-1.384 |
| C(ar)-N(4) | 0.0790 | 0.2000 | 0.1227 | 1.461-1.470 |
| C(ar)-N(3) | 0.0290 | 0.2841 | 0.2339 | 1.340-1.476 |
| C(ar)-N(2) | -0.0080 | -0.0087 | 0.0113 | 1.422-1.442 |
| C(sp ²)-N(3) (furoxan) | -0.0202 | -0.0213 | -0.0216 | 1.311-1.324 |

Continued on next page..

Table S1: Values of the Kullback-Leibler (KL) divergence of the different training sets and the tautobase at specific intervals for different types of bonds for molecules with $n_{\text{atoms}} \leq 9$. The values of the bond lengths were taken from Allen, F.H., *et al.*, 2006² (cont.)

| Type of Bond | QM9 | PC9 | ANI-1E | Interval (Å) |
|---------------------------------------------|---------|---------|---------|--------------|
| C(sp ²)-N(2) | -0.1046 | -0.0753 | -0.0409 | 1.273-1.339 |
| C(ar)-N(3) | -0.0897 | -0.0923 | -0.0962 | 1.325-1.369 |
| C(ar)-N(2) | -0.0807 | -0.0801 | -0.0853 | 1.300-1.348 |
| C(sp)-N(2) | 0.0131 | 0.0001 | 0.0024 | 1.140-1.148 |
| C(sp)-N(1) | -0.1771 | -0.2281 | -0.0925 | 1.131-1.449 |
| Carbon-Oxygen bonds | | | | |
| C(sp ³)-O(2) (Alcohols) | 0.7924 | 0.6993 | 0.7431 | 1.395-1.449 |
| C(sp ³)-O(2)(Dialkyl ethers) | 0.7733 | 0.6979 | 0.6591 | 1.405-1.458 |
| C(sp ³)-O(2)(aryl alkyl ethers) | 0.4180 | 0.4313 | 0.3602 | 1.417-1.438 |
| C(sp ²)-O(2) ¹ | 0.2570 | 0.1608 | 0.0713 | 1.435-1.501 |
| C(sp ²)-O(2)(Ring systems) | 0.3480 | 0.2537 | 0.1312 | 1.430-1.501 |
| C(sp ²)-O(2)(Enols) | -0.0370 | -0.0262 | -0.0359 | 1.324-1.342 |
| C(sp ²)-O(2)(enol esters) | -0.0516 | -0.0156 | -0.0380 | 1.341-1.363 |
| C(sp ²)-O(2)(acids) | -0.0245 | -0.0172 | -0.0248 | 1.279-1.320 |
| C(sp ²)-O(2)(esters) | 0.2340 | 0.1834 | 0.3607 | 1.328-1.420 |
| C(sp ²)-O(2)(anhydrides) | 0.0068 | -0.0116 | 0.0138 | 1.379-1.393 |
| C(sp ²)-O(2)(ring systems) | -0.0932 | -0.0388 | -0.0697 | 1.332-1.377 |
| C(ar)-O(2)(Phenols) | -0.0390 | -0.0100 | -0.0245 | 1.353-1.373 |
| C(ar)-O(2)(aryl alkyl ethers) | -0.0215 | -0.0096 | -0.0127 | 1.363-1.377 |
| C(ar)-O(2)(diaryl ethers) | -0.0010 | -0.0151 | 0.0059 | 1.375-1.391 |
| C(ar)-O(2)(esteres) | 0.1042 | 0.0453 | 0.1445 | 1.394-1.408 |

Continued on next page..

¹Aryl alkyl ethers, alkyl esters of carboxylic acids, alkyl esters of alpha, beta unsaturated acids, alkyl esterets of benzoic acid

Table S1: Values of the Kullback-Leibler (KL) divergence of the different training sets and the tautobase at specific intervals for different types of bonds for molecules with $n_{\text{atoms}} \leq 9$. The values of the bond lengths were taken from Allen, F.H., *et al.*, 2006² (cont.)

| Type of Bond | QM9 | PC9 | ANI-1E | Interval (Å) |
|----------------------------------------------------------|---------|---------|---------|--------------|
| C(sp ²)-O(1)(double) (Aldehydes and ketones) | -0.1119 | -0.1178 | -0.1090 | 1.188-1.238 |
| C(sp ²)-O(1)(double) ² | -0.0370 | -0.0513 | -0.0399 | 1.232-1.262 |
| C(sp ²)-O(1)(double)(carboxylic acids) | -0.0887 | -0.0917 | -0.0811 | 1.203-1.241 |
| C(sp ²)-O(1)(double)(esters) | -0.0477 | -0.0509 | -0.0523 | 1.181-1.207 |
| C(sp ²)-O(1)(anhydrides) | -0.0198 | -0.0164 | -0.0199 | 1.184-1.193 |
| C(sp ²)-O(1)(lactones) | 0.0000 | 0.0000 | 0.0000 | 1.187-1.209 |
| C(sp ²)-O(1)(double)(amides) | -0.1086 | -0.1185 | -0.1058 | 1.193-1.243 |
| Nitrogen-nitrogen bonds | | | | |
| N(4)-N(3) | -0.0109 | 0.0094 | 0.0150 | 1.412-1.418 |
| N(3)-N(3) | -0.1170 | 0.1075 | 0.2943 | 1.384-1.457 |
| N(3)-N(2) | 0.0426 | -0.1165 | -0.0721 | 1.345-1.375 |
| N(2)-N(2)(aromatic) | 0.2894 | -0.1551 | -0.1649 | 1.287-1.375 |
| N(2)-N(2) | 0.0477 | 0.0710 | -0.0100 | 1.202-1.262 |
| N(2)-N(1) (azides) | 0.0000 | 0.0203 | 0.0003 | 1.114-1.137 |
| Nitrogen-Oxygen bonds | | | | |
| N(3)-O(2) | 0.5630 | 0.1865 | 0.5170 | 1.388-1.468 |
| N(3)-O(1) | -0.1038 | -0.0670 | -0.0907 | 1.228-1.316 |
| N(2)-O(2) | 0.6880 | 0.0412 | 0.8593 | 1.365-1.420 |
| N(3)-O(1) | -0.0948 | 0.0117 | -0.0875 | 1.203-1.251 |

²Delocalized double bonds in carboxylate anions

Table S2: Values of the Kullback-Leibler (KL) divergence of the different training sets and the tautobase at specific intervals for different types of bonds for molecules with $n_{\text{atoms}} > 9$. The values of the bond lengths were taken from Allen, F.H., *et al.*, 2006³

| Type of Bond | QM9 | PC9 | ANI-1E | Interval(Å) |
|-------------------------------------------------|---------|---------|---------|-------------|
| C(sp)-C(sp)(triple) | 0.003 | 0.000 | 0.005 | 1.167-1.197 |
| C(sp ²)-C(sp ²)(double) | -0.121 | -0.022 | 0.000 | 1.280-1.405 |
| C(sp ²)-C(sp ²)(single) | 0.767 | 0.719 | 0.657 | 1.400-1.568 |
| C(sp ³)-C(sp ³)(single) | 0.937 | 0.853 | 0.746 | 1.458-1.610 |
| C(sp)-C(sp)(single) | -0.183 | -0.217 | -0.158 | 1.374-1.474 |
| C(ar)-C(ar) | -0.202 | -0.208 | -0.191 | 1.350-1.440 |
| C(sp ³)-C(sp ²) | 0.499 | 0.482 | 0.582 | 1.470-1.538 |
| C(sp ³)-C(ar) | 0.513 | 0.513 | 0.584 | 1.479-1.539 |
| C(sp ³)-C(sp) | -0.014 | -0.031 | 0.003 | 1.436-1.481 |
| C(sp ²)-C(ar) | 0.146 | 0.069 | 0.249 | 1.441-1.512 |
| C(sp ²)-C(sp) | -0.021 | -0.024 | -0.018 | 1.425-1.441 |
| C(ar)-C(sp) | -0.019 | -0.022 | -0.016 | 1.430-1.448 |
| Carbon-Nitrogen bonds | | | | |
| C(sp ³)-N(4) | 0.1634 | 0.0808 | 0.0236 | 1.482-1.510 |
| C(sp ³)-N(3) | 0.5185 | 0.6255 | 0.4057 | 1.446-1.572 |
| C(sp ³)-N(2) | 0.3322 | 0.4451 | 0.2122 | 1.461-1.506 |
| C(sp ²)-N(3) | -0.2625 | -0.2728 | -0.2479 | 1.314-1.419 |
| C(sp ²)-N(2) (Imidazole) | -0.0560 | -0.0593 | -0.0518 | 1.369-1.384 |
| C(ar)-N(4) | 0.0733 | 0.1890 | 0.1165 | 1.461-1.470 |
| C(ar)-N(3) | -0.0104 | 0.2425 | 0.1849 | 1.340-1.476 |
| C(ar)-N(2) | -0.0027 | -0.0028 | 0.0118 | 1.422-1.442 |
| C(sp ²)-N(3) (furoxan) | -0.0226 | -0.0240 | -0.0221 | 1.311-1.324 |

Continued on next page..

Table S2: Values of the Kullback-Leibler (KL) divergence of the different training sets and the tautobase at specific intervals for different types of bonds for molecules with $n_{\text{atoms}} > 9$. The values of the bond lengths were taken from Allen, F.H., *et al.*, 2006³ (cont.)

| Type of Bond | QM9 | PC9 | ANI-1E | Interval(Å) |
|---------------------------------------------|---------|---------|---------|-------------|
| C(sp ²)-N(2) | -0.0917 | -0.0424 | -0.0127 | 1.273-1.339 |
| C(ar)-N(3) | -0.0984 | -0.0977 | -0.1007 | 1.325-1.369 |
| C(ar)-N(2) | -0.0855 | -0.0850 | -0.0863 | 1.300-1.348 |
| C(sp)-N(2) | 0.0136 | 0.0005 | 0.0028 | 1.140-1.148 |
| C(sp)-N(1) | -0.1404 | -0.1741 | -0.0339 | 1.131-1.449 |
| Carbon-Oxygen bonds | | | | |
| C(sp ³)-O(2) (Alcohols) | 0.6515 | 0.5870 | 0.5996 | 1.395-1.449 |
| C(sp ³)-O(2)(Dialkyl ethers) | 0.6108 | 0.5655 | 0.5093 | 1.405-1.458 |
| C(sp ³)-O(2)(aryl alkyl ethers) | 0.3302 | 0.3556 | 0.2713 | 1.417-1.438 |
| C(sp ²)-O(2) ³ | 0.1719 | 0.0874 | 0.0270 | 1.435-1.501 |
| C(sp ²)-O(2)(Ring systems) | 0.2398 | 0.1593 | 0.0673 | 1.430-1.501 |
| C(sp ²)-O(2)(Enols) | -0.0349 | -0.0245 | -0.0335 | 1.324-1.342 |
| C(sp ²)-O(2)(enol esters) | -0.0418 | -0.0013 | -0.0211 | 1.341-1.363 |
| C(sp ²)-O(2)(acids) | -0.0261 | -0.0196 | -0.0271 | 1.279-1.320 |
| C(sp ²)-O(2)(esters) | 0.2461 | 0.2170 | 0.3624 | 1.328-1.420 |
| C(sp ²)-O(2)(anhydrides) | 0.0175 | -0.0017 | 0.0245 | 1.379-1.393 |
| C(sp ²)-O(2)(ring systems) | -0.0718 | -0.0090 | -0.0364 | 1.332-1.377 |
| C(ar)-O(2)(Phenols) | -0.0261 | 0.0091 | -0.0040 | 1.353-1.373 |
| C(ar)-O(2)(aryl alkyl ethers) | -0.0112 | 0.0045 | 0.0018 | 1.363-1.377 |
| C(ar)-O(2)(diaryl ethers) | 0.0114 | -0.0029 | 0.0192 | 1.375-1.391 |
| C(ar)-O(2)(esteres) | 0.1064 | 0.0513 | 0.1394 | 1.394-1.408 |

Continued on next page..

³Aryl alkyl ethers, alkyl esters of carboxylic acids, alkyl esters of alpha, beta unsaturated acids, alkyl esterets of benzoic acid

Table S2: Values of the Kullback-Leibler (KL) divergence of the different training sets and the tautobase at specific intervals for different types of bonds for molecules with $n_{\text{atoms}} > 9$. The values of the bond lengths were taken from Allen, F.H., *et al.*, 2006³ (cont.)

| Type of Bond | QM9 | PC9 | ANI-1E | Interval(Å) |
|---------------------------------------------------------|---------|---------|---------|-------------|
| C(sp ²)-O(1)(double) Aldehydes and ketones) | -0.1140 | -0.1154 | -0.1149 | 1.188-1.238 |
| C(sp ²)-O(1)(double) ⁴ | -0.0404 | -0.0553 | -0.0426 | 1.232-1.262 |
| C(sp ²)-O(1)(double)(Carboxylic acids) | -0.0978 | -0.0981 | -0.0938 | 1.203-1.241 |
| C(sp ²)-O(1)(double)(esters) | -0.0373 | -0.0375 | -0.0425 | 1.181-1.207 |
| C(sp ²)-O(1)(anhydrides) | -0.0143 | -0.0118 | -0.0150 | 1.184-1.193 |
| C(sp ²)-O(1)(lactones) | 0.0000 | 0.0000 | 0.0000 | 1.187-1.209 |
| C(sp ²)-O(1)(double)(amides) | -0.1143 | -0.1195 | -0.1149 | 1.193-1.243 |
| Nitrogen-Nitrogen bonds | | | | |
| N(4)-N(3) | -0.0088 | 0.0221 | 0.0297 | 1.412-1.418 |
| N(3)-N(3) | -0.0963 | 0.2138 | 0.4141 | 1.384-1.457 |
| N(3)-N(2) | 0.0599 | -0.1094 | -0.0745 | 1.345-1.375 |
| N(2)-N(2)(aromatic) | 0.2938 | -0.1645 | -0.1646 | 1.287-1.375 |
| N(2)-N(2) | 0.0053 | 0.0423 | -0.0506 | 1.202-1.262 |
| N(2)-N(1) (azides) | 0.0000 | 0.0203 | 0.0003 | 1.114-1.137 |
| Nitrogen-Oxygen bonds | | | | |
| N(3)-O(2) | 0.8954 | 0.4577 | 0.8386 | 1.388-1.468 |
| N(3)-O(1) | -0.1448 | -0.1724 | -0.1143 | 1.228-1.316 |
| N(2)-O(2) | 1.0017 | 0.1725 | 1.2526 | 1.365-1.420 |
| N(3)-O(1) | -0.1417 | -0.1208 | -0.1158 | 1.203-1.251 |

⁴Delocalized double bonds in carboxylate anions

Table S3: Mean Absolute (MAE) and Root-Mean-Squared Error (RMSE) for the prediction of tautomerization energy ΔE_{Tauto} , and the single isomer energies, E_{SI} , for the entire Tautobase (1257 tautomeric pairs) for each of the datasets evaluated for the MMFF94 force field geometries.

| Database | ΔE_{Tauto} | | E_{SI} | |
|----------|---------------------------|-------|-----------------|-------|
| | MAE | RMSE | MAE | RMSE |
| QM9 | 7.40 | 10.60 | 8.36 | 11.76 |
| PC9 | 6.59 | 9.72 | 9.65 | 14.95 |
| ANI-1E | 6.11 | 9.31 | 16.70 | 16.70 |
| ANI-1 | 5.57 | 8.79 | 20.17 | 30.35 |
| ANI-1x | 3.42 | 5.79 | 5.97 | 8.38 |

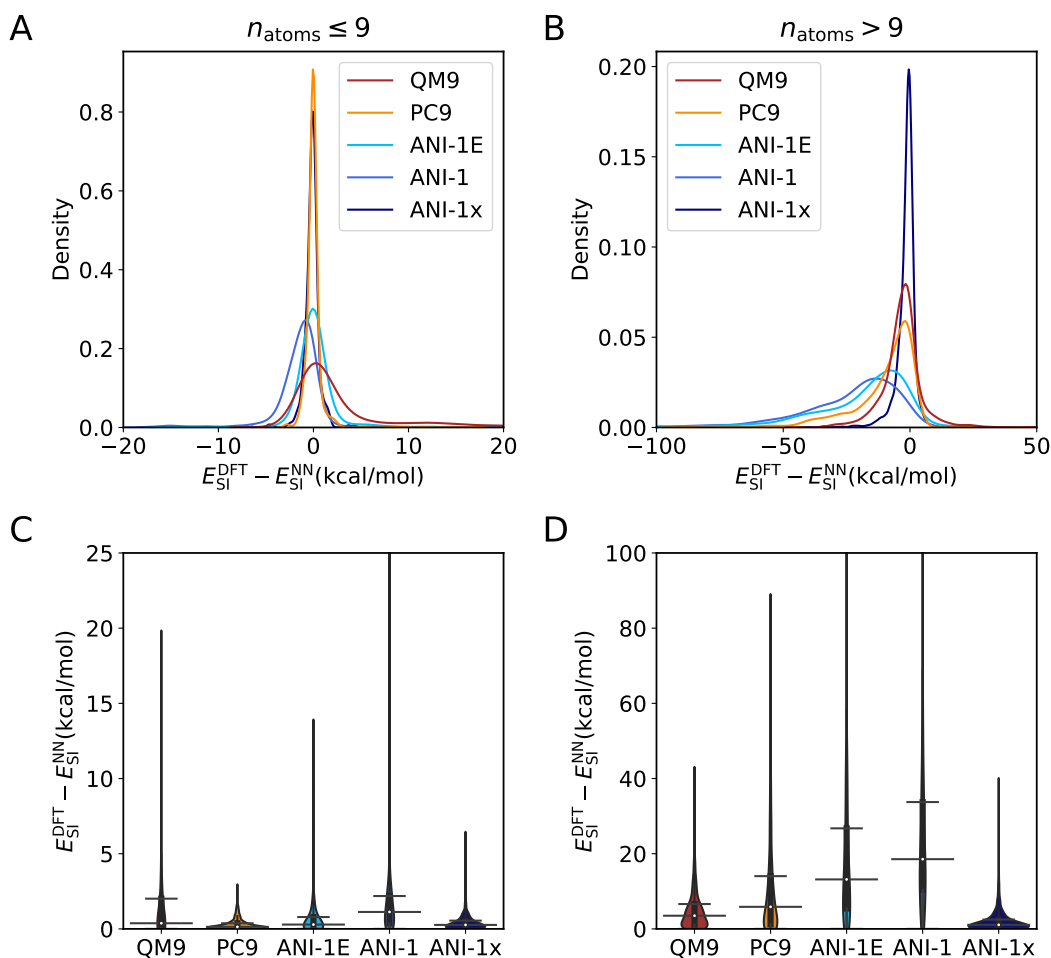


Figure S1: Error analysis on the prediction of energies of the single molecules. Panels A and B: Kernel density estimate for prediction of the energies of single isomer for the different databases. Panels C and D: Normalized error distribution up to the 95% quantile of the different datasets evaluated on this work for the energy of a single isomer. The blackbox inside spans between the 25% and 75% quantiles with a white dot indicating the mean of the distribution. The whisker marks indicate the 5% and 95% quantiles. The left and right columns are for Set1 and Set2, respectively.

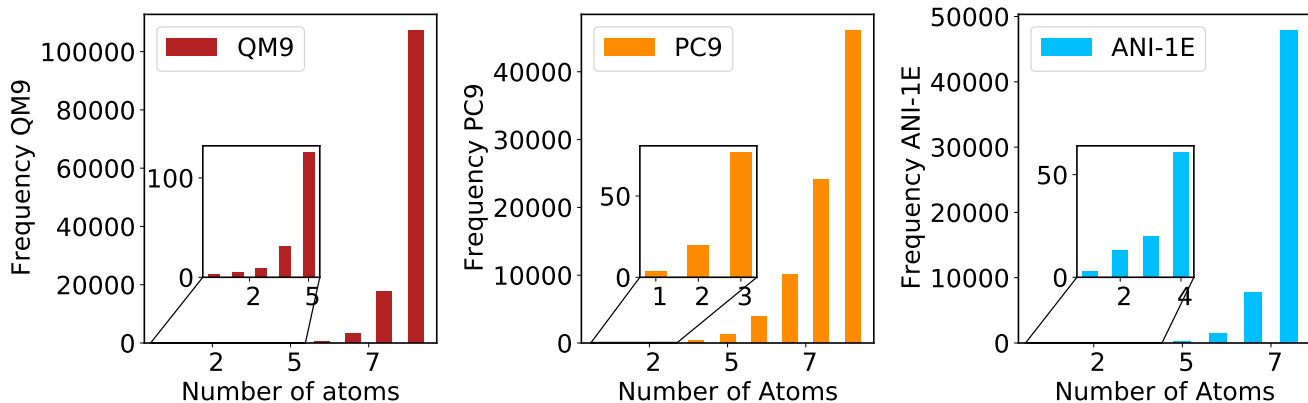


Figure S2: Number of heavy atoms (C,N,O) in the QM9, PC9, and ANI-1E databases (from left to right) used in the present work. The insets show enlargements for cases with few representatives.

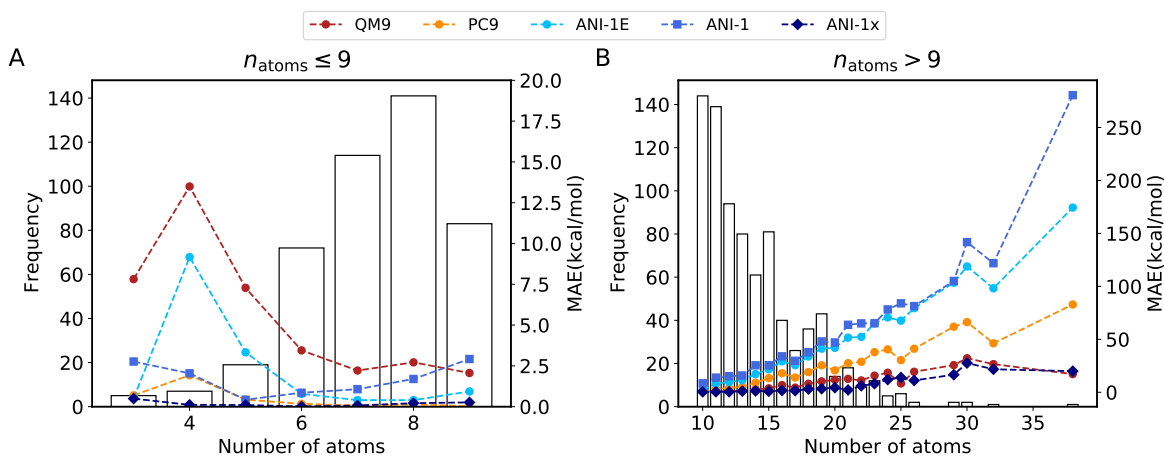


Figure S3: Mean Absolute Error (MAE) by number of heavy atoms (C,O,N) for E_{SI} . A histogram of the number of molecules for different numbers of heavy atoms n is shown in the background. Panel A for Set1 and panel B for Set2.

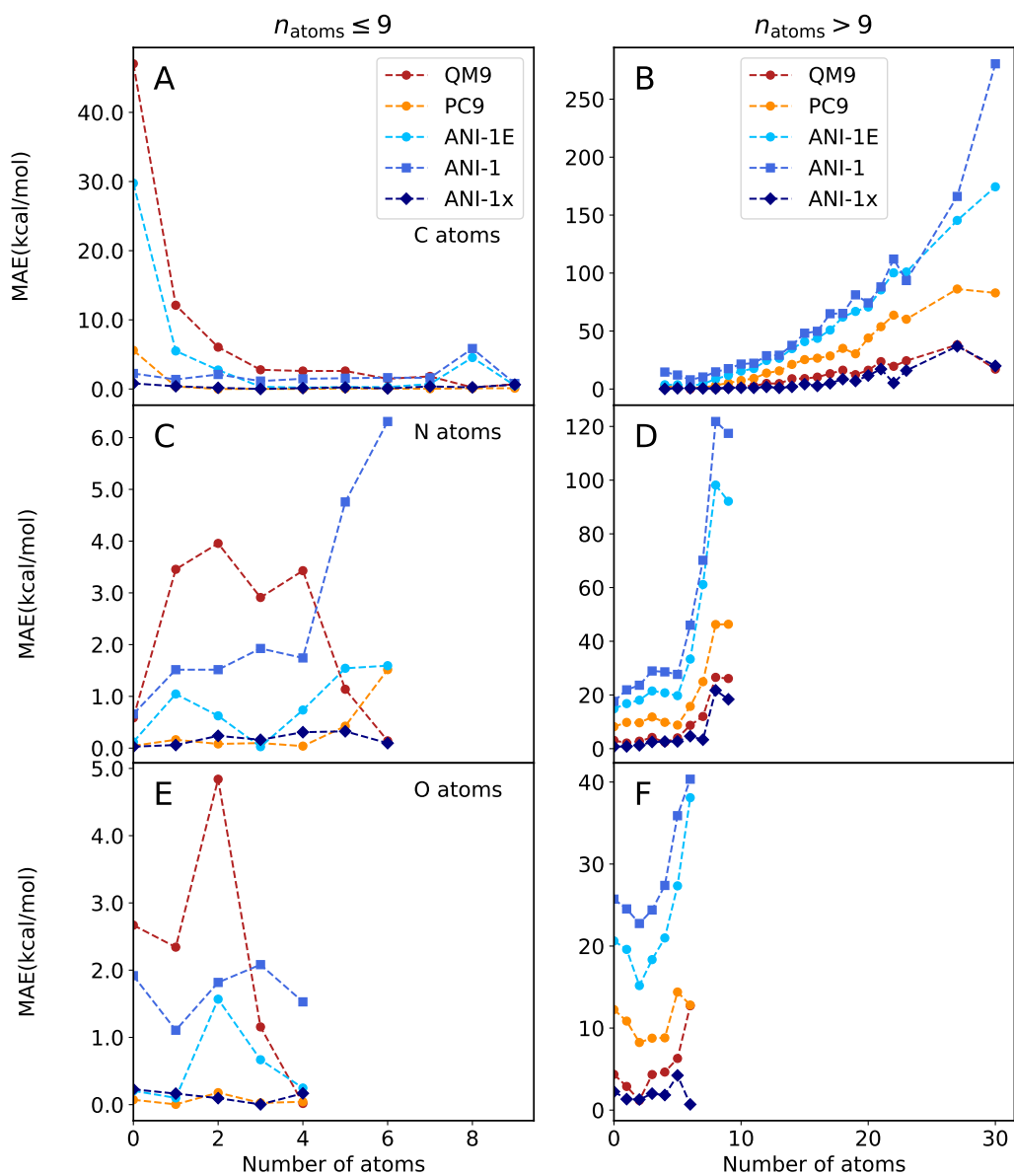


Figure S4: Mean Absolute Error (MAE) by number of atoms of a given element (carbon (top), nitrogen (middle), oxygen (bottom)) for the energy of a single isomer E_{SI} . Panels A and B shows the results by number of C atoms. Panels C and D shows the results by number of N atoms. Finally, panels E and F show the results by number of O atoms. Left and right columns for Set1 and Set2, respectively.

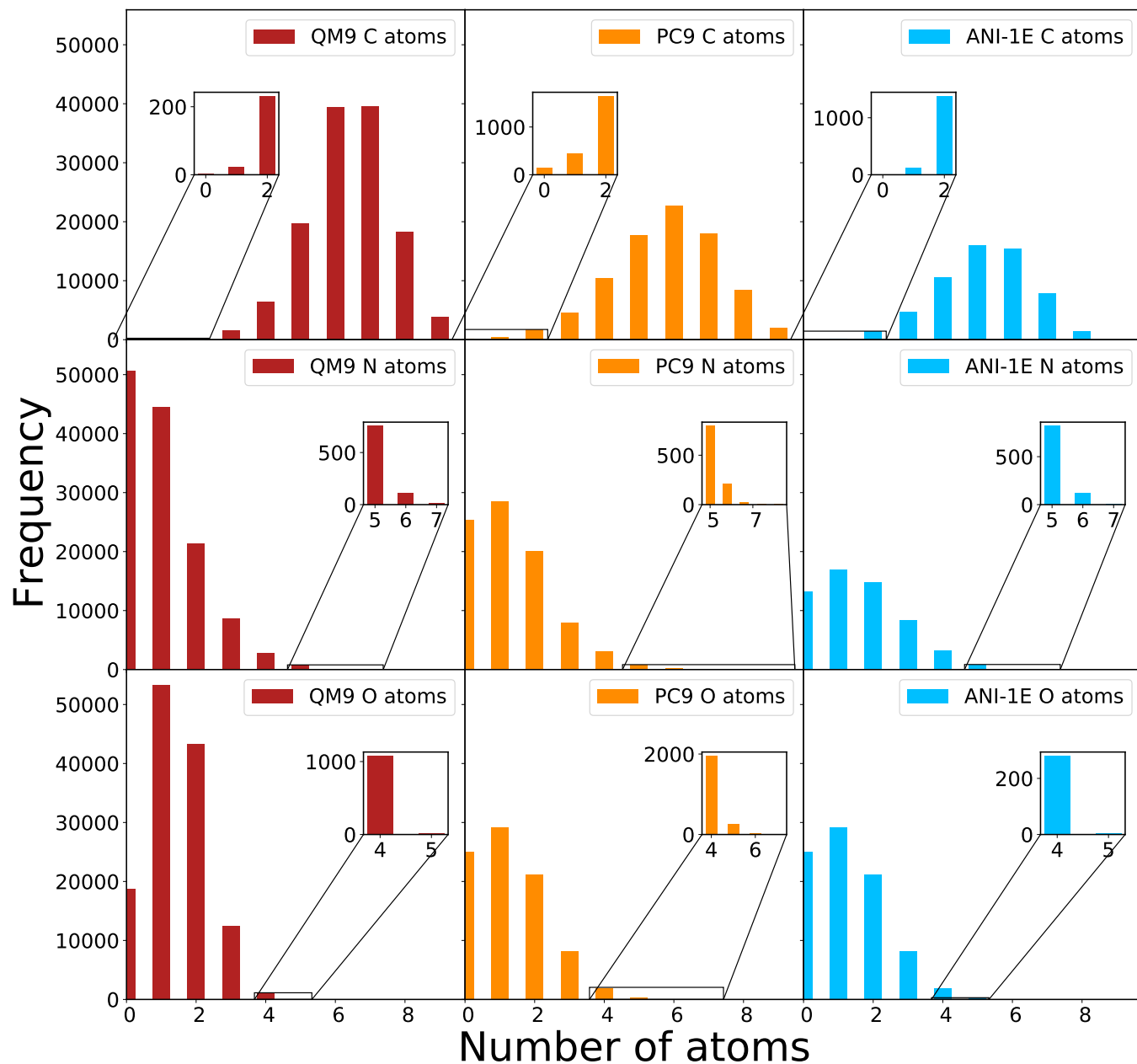


Figure S5: Number of C-, N-, and O- atoms (from top to bottom) in the QM9, PC9, and ANI-1E databases (from left to right) used in the present work. The insets show enlargements for cases with few representatives.

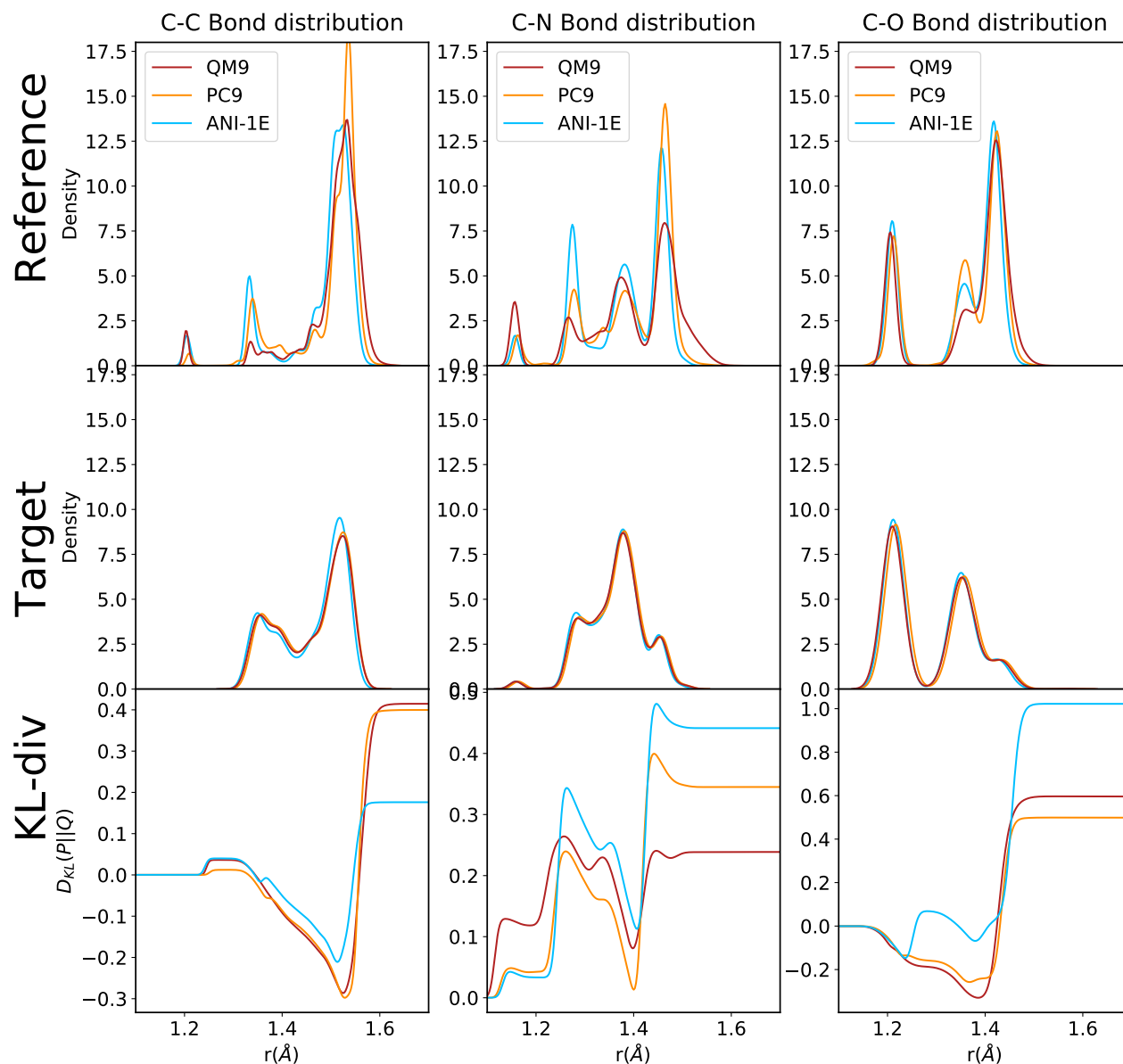


Figure S6: Kernel distributions of different types of bond lengths involving C atoms. Top row are the results for the reference sets (PC9, QM9 and ANI-1E). Middle row shows the results of the geometries of tautobase optimized at level of theory of the different databases for Set1. The KL-divergence between reference and target data set distributions is reported in the bottom row.

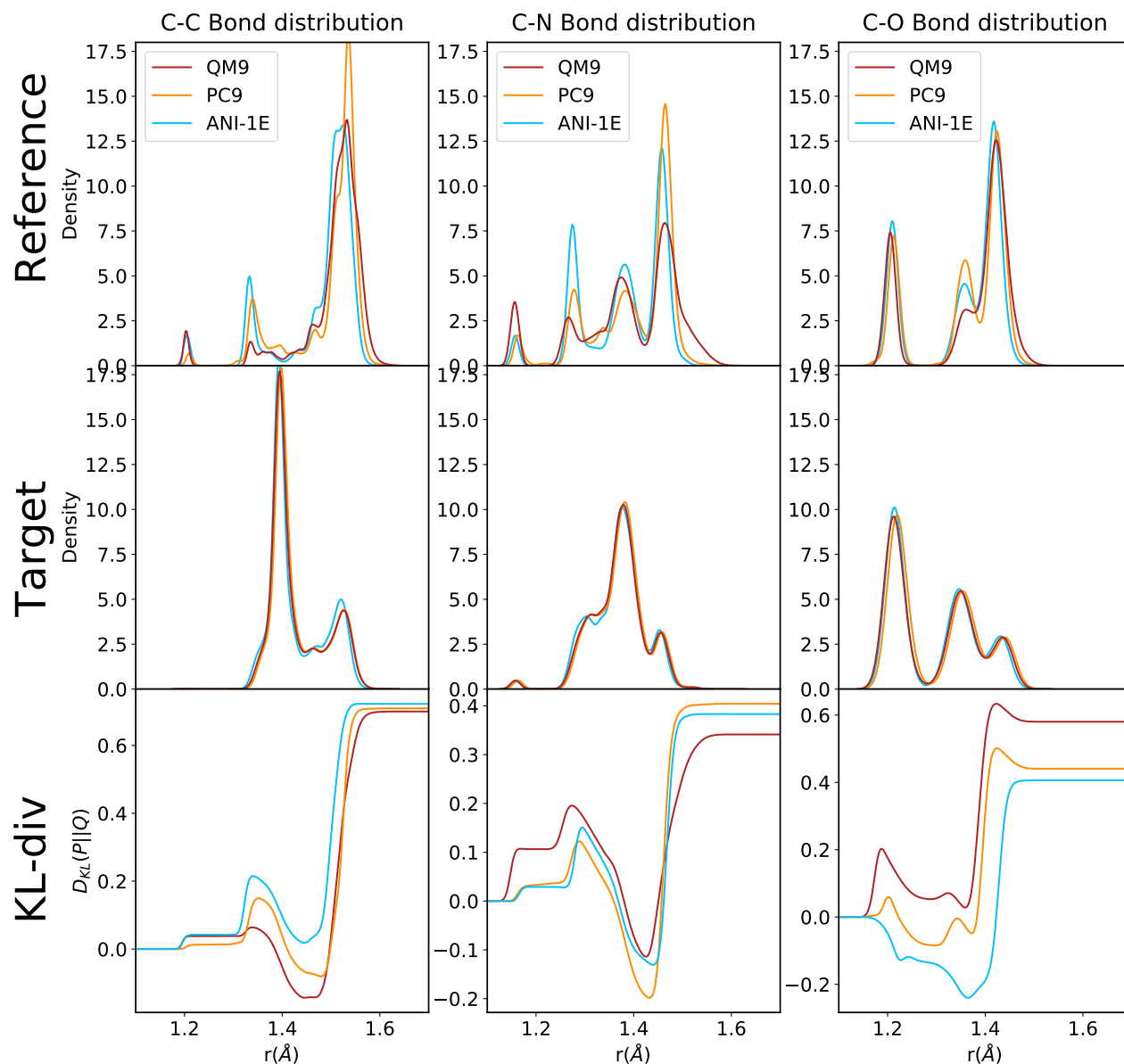


Figure S7: Kernel distributions of different types of bond lengths involving C atoms. Top row are the results for the reference sets (PC9, QM9 and ANI-1E). Middle row shows the results of the geometries of tautobase optimized at level of theory of the different databases for Set2. The KL-divergence between reference and target data set distributions is reported in the bottom row.

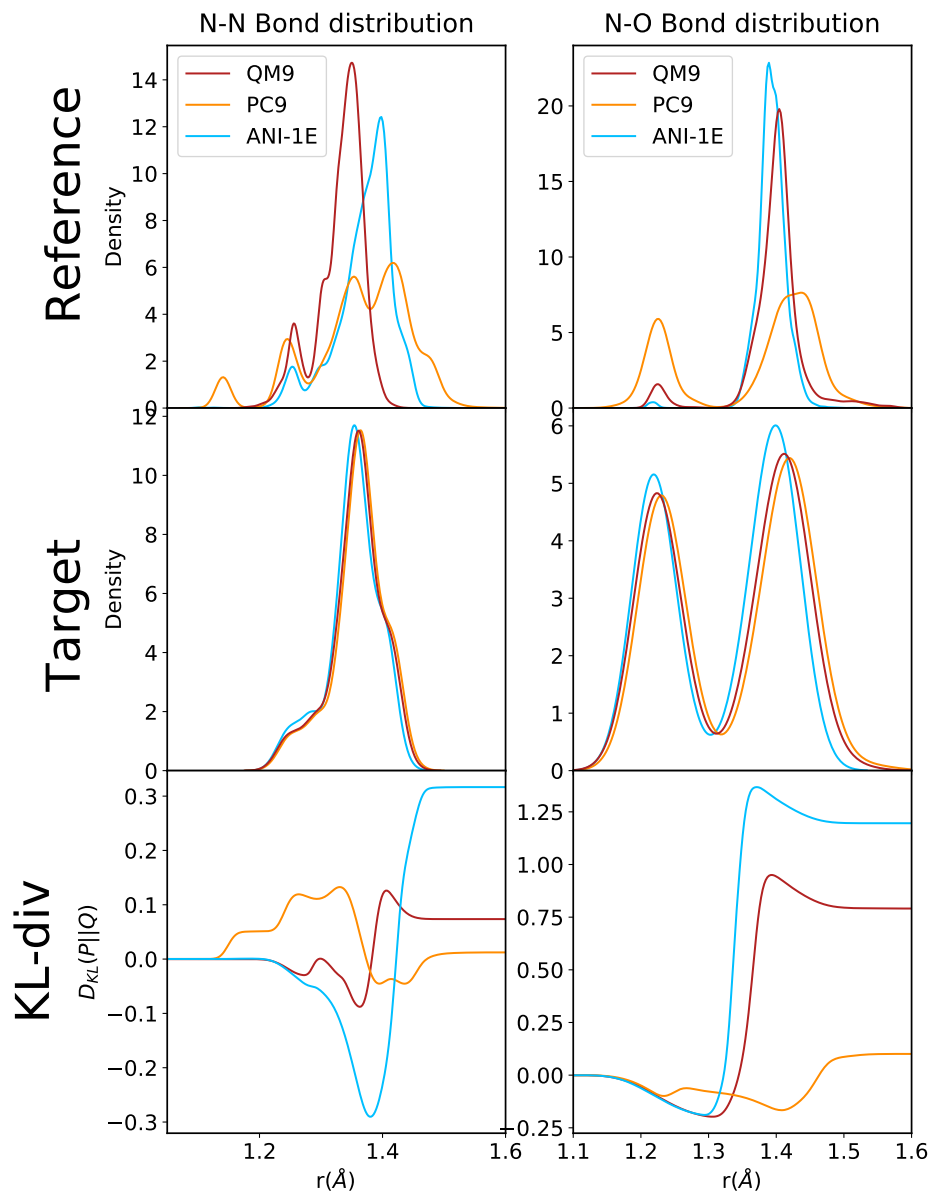


Figure S8: Kernel distributions of different types of bond lengths involving N atoms. Top row are the results for the reference sets (PC9, QM9 and ANI-1E). Middle row shows the results of the geometries of tautobase optimized at level of theory of the different databases for Set1. The KL-divergence between reference and target data set distributions is reported in the bottom row..

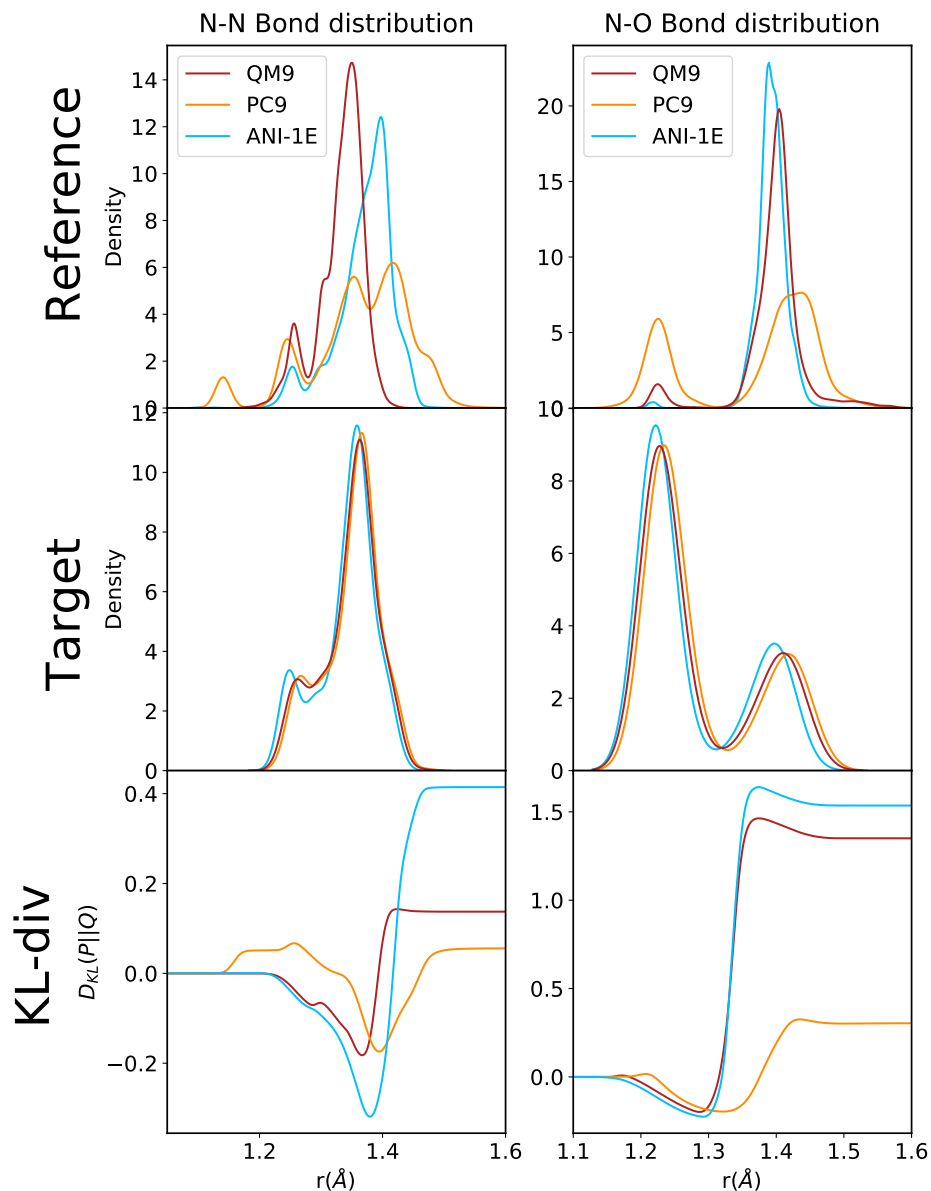


Figure S9: Kernel distributions of different types of bond lengths involving C atoms. Top row are the results for the reference sets (PC9, QM9 and ANI-1E). Middle row shows the results of the geometries of tautobase optimized at level of theory of the different databases for Set2. The KL-divergence between reference and target data set distributions is reported in the bottom row.

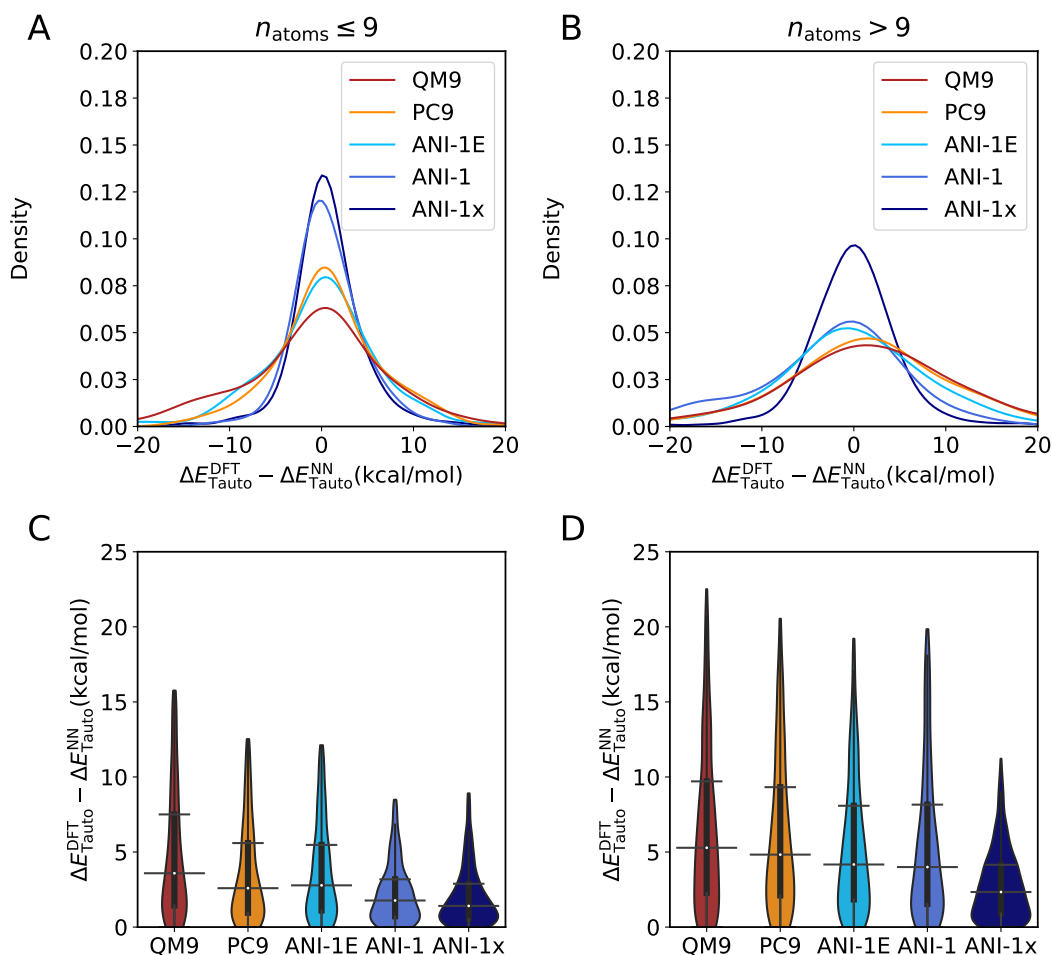


Figure S10: Error analysis on the prediction of the tautomerization energies using an optimized geometry with MMFF94 force field. Panels A and B: Kernel density estimate for prediction of the tautomerization energies for the different databases. Panels C and D: Normalized error distribution up to the 95% quantile of the different datasets evaluated on this work for the tautomerization energy. The blackbox inside spans between the 25% and 75% quantiles with a white dot indicating the mean of the distribution. The whisker marks indicate the 5% and 95 % quantiles. The left and right columns are for Set1 and Set2, respectively

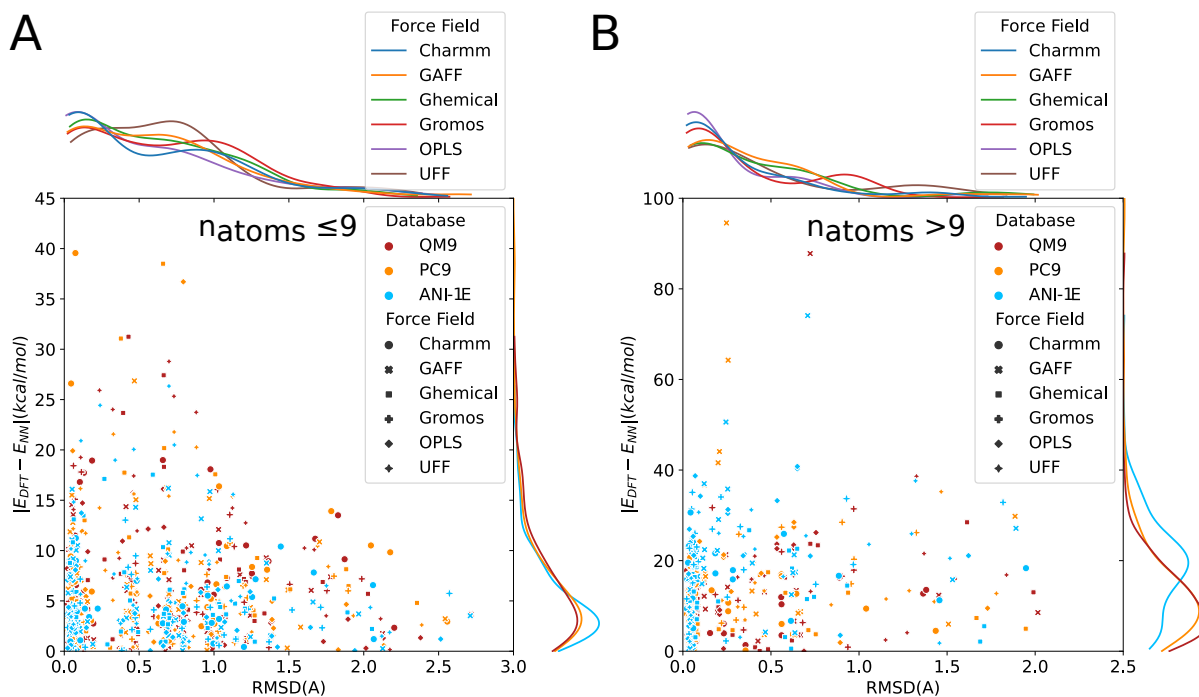


Figure S11: Effect of the initial geometry on the prediction of the energy by the NN models for the molecules from the SAMPL2 challenge.[?] Plots of the Root Mean Square Displacement with respect to the optimized geometry vs. the absolute error between the energy obtained from DFT calculations and the energy from the NN model for the molecules on panel A results for isomers with $n_{\text{atoms}} \leq 9$ and on panel B for $n_{\text{atoms}} > 9$. In both plots, the X axis shows the kernel distribution function for the RMSD for the different force fields used to generate the test geometries. In the Y axis is shown the Kernel distribution function for the predicted energies with the different databases.

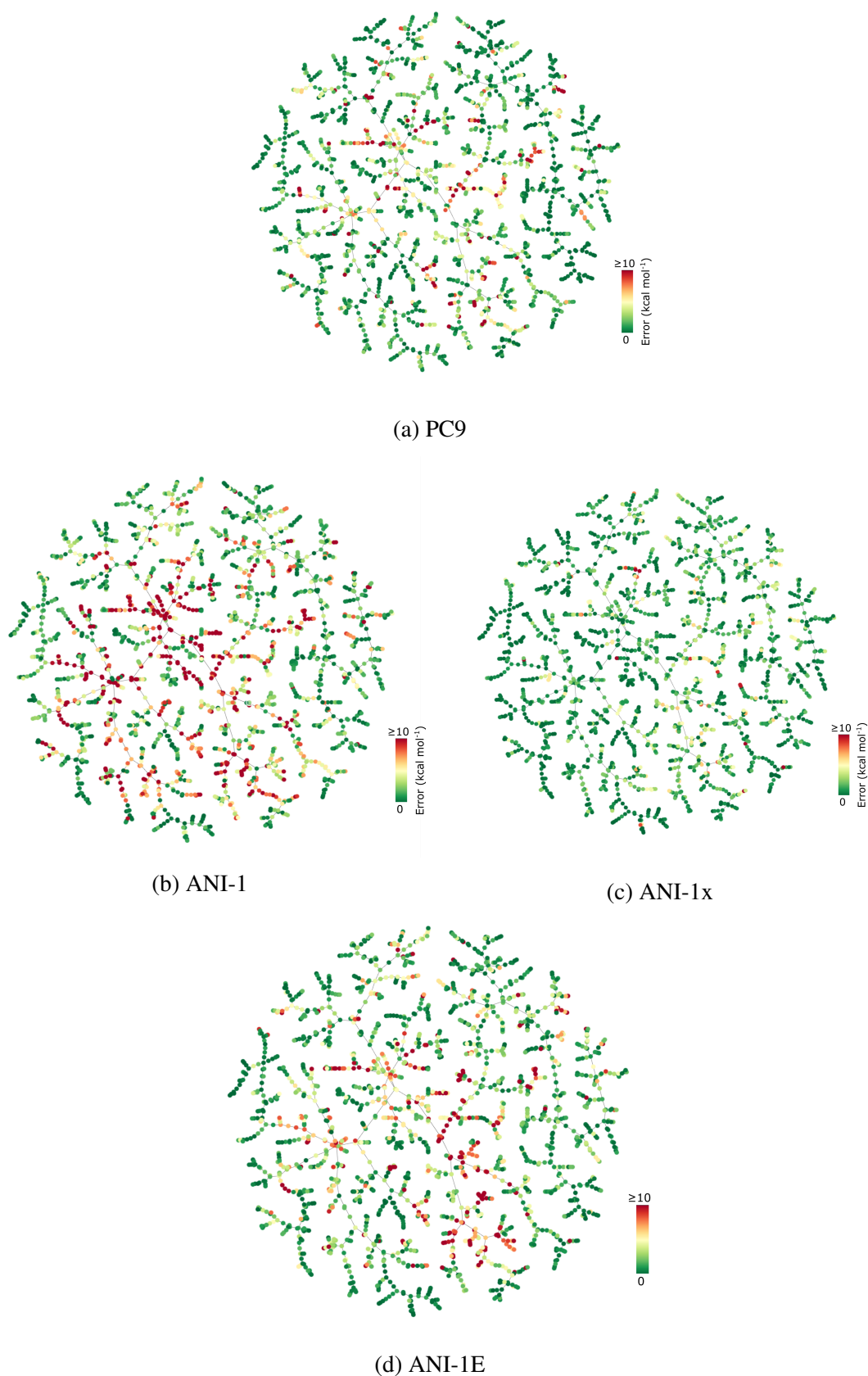


Figure S12: TMAP projection of chemical space for all molecules in the TautoBase, coloured by error in tautomerization energy calculated using the ML potentials trained on (a) PC9, (b) ANI-1, (c) ANI-1x and (d) ANI-1E.